Article ID: 1006-8775(2023)04-0410-21

Evaluation of Performance of Polar WRF Model in Simulating Precipitation over Qinghai-Tibet Plateau

XUE Jian-jun (薛建军)^{1,2}, XIAO Zi-niu (肖子牛)²

(1. China Meteorological Administration Training Centre, Beijing 100081 China; 2. State Key Laboratory of Numerical Modeling for Atmospheric Sciences and Geophysical Fluid Dynamics, Institute of Atmospheric Physics, Chinese Academy of Sciences, Beijing 100029 China)

Abstract: Considering the complex topographic forcing and large cryosphere concentration, the present study utilized the polar-optimized WRF model (Polar WRF) to conduct downscaling simulations over the Qinghai-Tibet Plateau (TP) and its surrounding regions. Multi-group experiments with the 10 km horizontal resolution are used to evaluate the modeling of precipitation. Firstly, on the basis of the model ground surface properties upgrade and the optimized Noah-MP, the "better-performing" configuration suite for modeling precipitation is comprehensively examined. Various model parameters such as nudging options, five cumulus parameterization schemes, two planetary boundary layer schemes, and six microphysics schemes are investigated to further refine the Polar WRF configuration. Moreover, the precipitation simulation for a full calendar year is compared with multiple reanalyses and observations. The simulations demonstrate that the Polar WRF model successfully captures the general features of precipitation over this region and is sensitive to model parameters. Based on the results, it is recommended to use grid nudging with q intensity coefficient of 0.0002, the multi-scale kain-fritsch cumulus parameterization, the Yonsei University boundary layer scheme, and the Morrison 2-mom microphysics with reduced default droplet concentration value of 100 cm⁻³. Overall, the model performance is better than the ERA-interim and TRMM 3b42. It is comparable to, and in some cases slightly better than, the CRA-Land, especially in the prediction for the western part of the plateau where in situ observations are limited, and the cryosphere-atmosphere interaction is more pronounced.

Key words: Polar WRF; precipitation; Qinghai-Tibet Plateau; downscaling simulations; parameter optimization **CLC number:** P456.7 **Document code:** A

Citation: XUE Jian-jun, XIAO Zi-niu. Evaluation of Performance of Polar WRF Model in Simulating Precipitation over Qinghai-Tibet Plateau [J]. Journal of Tropical Meteorology, 2023, 29(4): 410-430, https://doi.org/10.3724/j.1006-8775.2023.031

1. INTRODUCTION

The Qinghai-Tibet Plateau (TP), an area covering 2.5 million km² and an average elevation exceeding 4000 m, is the largest and the highest plateau on the earth (Bibi et al. [1]; Chen et al. [2]; Gao et al. [3]; Kang et al. [4]; Li et al. [5]; Tong et al. [6]). To some extent, the plateau is like a huge high mountain system, which is composed of mountains, plateaus, and rivers and interspersed with extensive broad valleys, basins, and lakes. Besides the extremely complex and various terrain, there are also a large number of glaciers covered by vast amounts of permafrost and snow, which rank third except for the Antarctic and Arctic (Kang et al. [4]; Yang et al. [7]; Yao et al. [8]; You et al. [9]). Hence, the Qinghai-Tibet Plateau was also known as the "Third Pole" (Bibi et al. [1]; Chen et al. [2]; Gao et al. [3]; Kang et

Received 2023-03-16; **Revised** 2023-08-15; **Accepted** 2023-11-15

Funding: National Natural Science Foundation of China (91937000, 91637208)

Biography: XUE Jian-jun, Ph.D., primarily undertaking research on climate prediction and weather forecast using numerical models.

Corresponding author: XIAO Zi-niu, e-mail: xiaozn@lasg.iap.ac.cn

al. [4]; Li et al. [5]; Tong et al. [6]; You et al. [9]; Li et al. [10]; Sun et al. [11]; Yao et al. [12]; Yao et al. [13]). TP plays a crucial role in the earth's climate system and acts on East Asia, even global weather and climate. Many excellent studies have confirmed that the forcing of the TP's significant dynamic and thermal effects change the difference between land and sea, affect atmospheric circulation, modulate the East Asian Monsoon, South Asian Monsoon, and the midlatitude westerly and their synergistic effects (Kang et al. [4]; You et al. [9]; Chen et al. [14]; Chen et al. [15]; Chen et al. [16]; Duan et al. [17]; Duan and Wu [18]; Jiang et al. [19]; Kuang et al. ^[20]; Lai et al. ^[21]; Liu et al. ^[22]; Liu et al. ^[23]; Wang et al. ^[24]; Wang et al. ^[26]; Wu et al. ^[27]; Wu et al. [28]; Ye [29]; Zhang et al. [30]; Zhou et al. [31]). Moreover, the significant processes of ice/snow and water cycle on TP can exert strong coupling processes, especially the coupling interaction of cryosphere-hydrosphereatmosphere with other spheres in the Earth system. It is believed to have a huge influence on regional and global weather climate and ecological environment (Bibi et al. [1]; Kang et al. [4]; Yao et al. [8]; You et al. [9]; Li et al. [10]; Yao et al. [12]; Chen et al. [14]; Liu et al. [22]; Zhang et al. [30]; Chan et al. [32]; Li et al. [33]).

It is very highly confident that the TP has been warming and wetting since the 1950s, and this trend beganto accelerate after the 1980s, which was indicated by

multiple facts (Bibi et al. [1]; Kang et al. [4]; Li et al. [10]; Yao et al. [12]; Chen et al. [14]; Kuang et al. [20]; Zhang et al. [30]; Chan et al. [32]; Li et al. [34]; Wu et al. [35]; Yang et al. [36]: You et al. [37]). To better understand these evident changes, the precipitation variations over TP were one of the key concerns for the research front (Kang et al. [4]; Yang et al. [7]; Yao et al. [8]; Yao et al. [12]; Wang et al. [24]; Wang et al. ^[26]; Arias et al. ^[38]; Chen et al. ^[39]; Cuo et al. ^[40]; Ning et al. ^[41]; Wang et al. ^[42]; Zhu et al. ^[43]; Zhu [44]). Numerical models have been widely used to investigate precipitation variations. Therefore, many studies have been devoted to improve the performance of precipitation simulation. The terrain/land use, the cumulus parameterization scheme (CUs), the planetary boundary layer parameterization scheme (PBLs), and cloud microphysical parameterization schemes (MPs) in numerical simulations, including the sensitivity to the accuracy of the precipitation have also been investigated (Gao et al. [3]; Li et al. [5]; Wang et al. [24]; Chen et al. [45]; Chen et al. [46]; Fu et al. [47]; Gao et al. [48]; You et al. [49]; Li et al. [50]; Lin et al. [51]; Norris et al. [52]; Ou et al. [53]; Tong et al. [54]; Wang et al. [55]; Wu et al. [56]; Xu et al. [57]; Yu et al. [58]). However, there are still few studies on the comprehensive optimization of multiple parameters with the same model version for a large area over the TP and the surrounding regions. In addition, due to the special characteristics, the precipitation mechanism and its evolution process in this region appear more complicated, especially under the rapid retreat of the cryosphere that has huge effects and feedback on surface energy balance, water vapor flux, clouds, etc. (Kang et al. [4]; Yang et al. [7]; Yao et al. [8]; You et al. [9]; Yao et al. [12]; Niu et al. [59]; Pepin et al. [60]). It still faces challenges for numerical models and reanalysis to describe the precipitation over TP (e.g., Tong et al. [6]; Chen et al. [45]; Bai et al. [61]; Liu et al. [62,63]; Wang et al. [64]). One factor contributing to these uncertainties is associated with the coupled processes of the special topographic forcing and the interaction of strong ice/snow-atmospheric feedbacks.

To the sophisticated description of "polar environmental characteristics" over TP, such as better heat transfer for ice/snow and more suitable model settings. Here, the polar-optimized WRF model V4.1.1 (Polar WRF) is used for downscaling simulations over the TP and its surrounding regions. This study aims to (1) investigate the impacts of multiple options to study the "better-performing" configuration suite enhancing the accuracy and reliability representation of precipitation for using Polar WRF; (2) generally evaluate whether precipitation can be reasonably simulated with this polaroptimized model over the TP by a full calendar year and thus are more statistically robust than sensitivity test and case studies. This investigation is also an extension of the utilization and test of the Polar WRF (V4.1.1) beyond the Antarctic and Arctic (Xue et al. [65,66]). It follows the series of verification studies documenting ongoing Polar WRF comprehensive evaluations and focuses on the "hottest topics" of modeling precipitation over the TP. The next sections are organized as follows: Section 2 concentrates on the Polar WRF model description. Section 3 depicts the experiments, model configuration, and data used in this study. The results of the simulation are performed in Section 4. Finally, the conclusion and discussion are provided in Section 5.

2. MODEL AND CONFIGURATIONS

2.1 Polar WRF

The polar version of the regional WRF model named "Polar WRF" is being developed, tested, and applied to climate variability and change problems in polar regions (e.g., Xue et al. ^[65]; Bromwich et al. ^[67,68,69]; Hines ^[70]; Hines and Bromwich ^[71]; Wilson et al. ^[72,73]). Polar WRF is based on the standard WRF (ARW) and has been improved by the Polar Meteorology Group at the Byrd Polar and Climate Research Center of Ohio State University. The primary task of the modifications is to make the model keep state-of-the-art skills in operational weather forecasting and research simulation over polar regions (Xue et al. [66]; Bromwich et al. [67]; Wilson et al. [72,73]; Kumar et al. [74]; Powers et al. [75,76]; Walsh et al. [77]). Hence, it focuses on the "polar environmental characteristics" such as optimizing heat transfer for ice sheets and revised surface energy balance in the Land Surface Model (LSM), comprehensively describing the ice, snow process, and optimal treatment of the ice/snowair feedback, improving and testing cloud microphysics for polar conditions. The improvements are present in different Polar WRF versions, and some are also absorbed by the rolling update of standard WRF (Xue et al. [65]; Bromwich et al. [68,69]; Hines et al. [71,70][78,79]; Hines and Bromwich [80]).

Upon the release of WRF 4.X, the Polar WRF was pushed to V4.1.1 in 2019 with the significant new features modified Noah-MP and the improvement in the downward shortwave radiation implemented that compared with the Polar WRF V3.X. This version of the model serves good performance both in the Antarctic and Arctic. The results of the benchmark over the Antarctic and the Southern Ocean indicate that the model has good skills for variables, including surface and vertical of the atmosphere, for intraannual variations in large-scale atmospheric circulation (Xue et al. [65]). For the polar mesoscale system, the model was applied over the Arctic region by simulating polar lows that demonstrated good performance (Xue et al. [66]). Considering the model performance under multiple polar conditions and the better utilization experience needed to investigate further, the Polar WRF V4.1.1 is continuously utilized in this study.

2.2 Model land static data upgrade

Topography, land cover, and vegetation can have significant impacts on processes such as orographic drag, albedo, radiation, surface roughness, soil temperature, and humidity, which play crucial roles in the heat and moisture fluxes conduction and exchange between the land surface

and atmosphere (Skamarock et al. [81]). Finer represents the land surface information such as terrain, land use, and vegetation in regional models is highly confident of improving model skills (Cao et al. [82]; Li et al. [83]; Li et al. [85]; Nahian et al. [86]; Schicker et al. [87]; Teklay et al. [88]; Yin et al. [89]). To better capture the characteristics over TP, the new terrain and land use are used to replace the default static data that was released with the model. The SRTM (Shuttle Radar Topography Mission) (Farr et al. [90]) 3 arc-second digital elevation data (the spatial resolution of the data is ~90 m×90 m) is applied (Fig. 1) to replace the SRTM 30 arc-second terrain data (spatial resolution of ~900 m×900 m) (De Meij et al. [91]). Even on a grid with a horizontal resolution of 10 km, there are significant differences (exceeding±300m) between the two in steep mountain areas of the TP. More refined land use data of TP from the National Tibet Data Center (TPDC) (Xu [92]), with a spatial resolution of 300 m×300 m, to optimize the model's default land use (Schicker et al. [87]). Compared with the original land use, the classification of permafrost and tundra has been added to the land surface data, and the main distribution areas are the Altun Mountains and the Kunlun Mountains in the northern part of TP. In addition, the representation of the land surface, such as the water body (lakes), ice, and snow on the plateau, also can be more vivid (figure not shown). 2.3 Model configuration

The model sets a single domain with 360×300 grid points on the Lambert projection (centered at 32.5°N, 87.5°E) and 10 km horizontal resolution, which covers the TP and its surrounding regions in western China (Fig. 1). In the vertical direction, the model utilizes HVC

hydrostatic pressure coordinates with 71 vertical levels and reaches the top of 3 hPa, as it has been noticed that a higher model top provides better treatment of upward propagating gravity waves (e.g., Xue et al. ^[65]; Wilson et al. ^[73]; Bromwich et al. ^[93]). The optimized Noah-MP (Xue et al. ^[65]) is used for the LSM to sufficiently perform land-atmosphere interaction. The Rapid Radiative Transfer Model (RRTMG) (Iacono et al. ^[94]) is selected for longwave and shortwave radiation that relies upon a wide range of previous tests (e.g., Xue et al. ^[65]; Bromwich et al. ^[67,68,69]; Hines and Bromwich ^[71], Wilson et al. ^[72]). There are more variations for other physical processes and closely related to sensitive tests. The details will be discussed in the next section.

Here, the monthly running method is carried out to better take into account the impacts of external forcing on the regional climate (Xue et al. [65]). However, to pursue a more economical way, the spin-up time is shortened to 5 days: that is, the model runs continuously for 33-36 days per month and outputs 3 hours at 0000, 0300, 0600, 0009, 0012, 0015, 0018, 0021 UTC for each day. The first 5 days at 0000 UTC before the 1st of each month are used for the mode spin-up, and the rest are the simulation results. The ERA-Interim (Dee et al. [95]) 60 model levels reanalysis is employed to initialize and drive model runs as the higher vertical resolution driving data showed better performance than those of less such as ERA5 (Hersbach et al. [96]) with 37 pressure vertical levels (Xue et al. [65]). As the reanalysis did not resolve the lakes over the TP. it is often recommended to solve the "hot lake" issue by the average surface air temperature used to adjust the lake surface temperature instead of the default that was

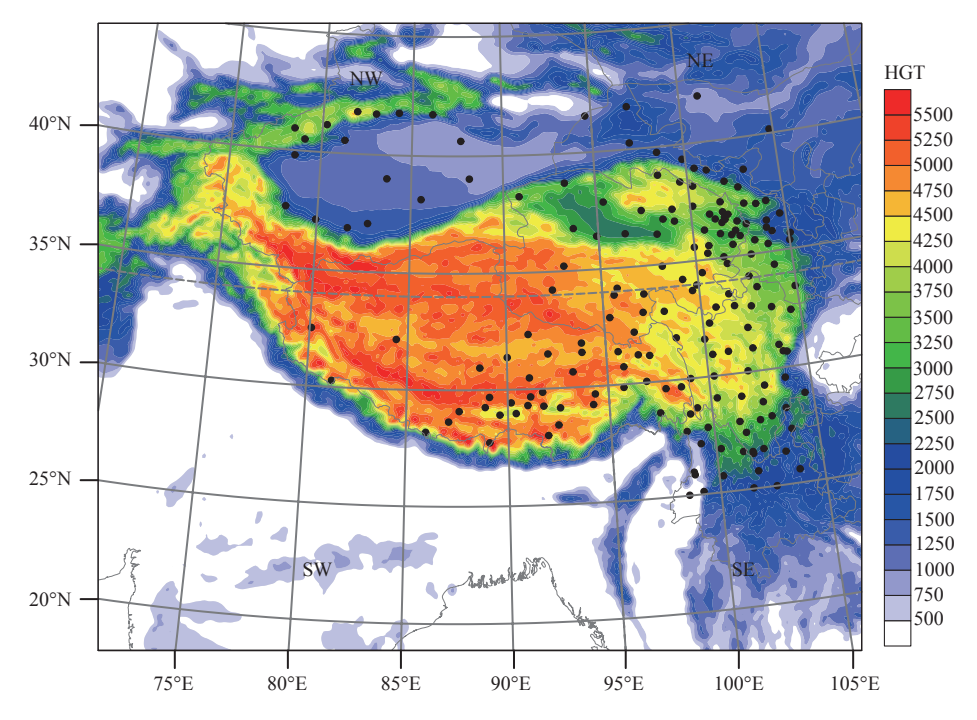


Figure 1. Model domain overlaid SRTM 3 arc-second terrain data at 10 km resolution. The black dots indicate the location of the in situ observations from TPDC. The gray dash lines along at 34°N and 95°E are used to divide the domain into four sub-regions (NW, Northwest; NW, Northeast; SE, Southeast; SW, Southwest).

extrapolated from the nearest resolved water bodies (e.g., Gao et al. [97]; Heath et al. [98]).

3. EXPERIMENTS

3.1 Numerical experiment design

One target of this study is to investigate the impacts of multiple options on the precipitation over TP and the surrounding regions. Considering configurations are highly correlated with each other; therefore, based on land static data optimization and the optimized Noah-MP, 4 categories of 19 sensitive experiments are comprehensively examined to further discuss the model performance, including the nudging setting, 5 CUs, 2 PBLs, and 6 MPs. All these numerical experiments are carried out in 2015 because more in situ observation and the new land use over TP from the TPDC are available during this period. Table 1 shows the summary for each experiment.

Nudging can force the model simulation towards a series of analyses grid-point by grid-point (Skamarock et al. [81]), which is used to reduce model drift (e.g., Xue et al. [65]; Bromwich et al. [67]; Hines et al. [79]; Glisan et al. [99]), particularly for simulations of extended periods (e.g., months). Inherited from the WRF, Polar WRF can afford to nudge u, v, t, and q from driving fields with spectral and grid nudge methods. Previous studies have shown that model skills are very sensitive to nudge settings when long-term runs or dynamic aspects need to be addressed (Xue et al. [66]; Cha et al. [100]; Liu et al. [101], Otte et al. [102]; von Storch et al. [103]). Therefore, the 6 experiments (nudging category in Table 1) for methods and nudging coefficients are investigated to increase the knowledge of nudging settings.

Several excellent investigations have identified that CUs schemes have a considerable impact on the simulation of precipitation over TP and nearby areas (Gao et al. [3]; Gao et al. [48]; You et al. [49]; Lin et al. [51]; Ou et al. [53]; Wu et al. [56]; Yu et al. [58]; Gao et al. [97]; Chen et al. [104]; Gao et al. [105]; Qian et al. [106]; Zheng et al. [107]). Referring to these findings, here we mainly study the influence of CUs settings by the following 3 typical kinds of simulation (a total of 5 experiments). (1) The Grell-Devenyi Ensemble Scheme (GD) and its improved version Grell-3 scheme (Grell et al. [108]). The GD combines multiple schemes and variants run within each grid point and gives an average feedback result. Currently, each grid box has 144 members in this scheme. Grell-3 (G3) is based on GD and is especially suitable for high-resolution simulations that should not be coarser than 10 km (Skamarock et al. [81]). (2) Kain-Fritsch schemes, including the Modified Kain-Fritsch (KF) (Kain [109]) and Multi-Scale Kain-Fritsch (MKF) (Zheng et al. [107]). KF using the mass flux with downdrafts and CAPE removal time scale for deep and shallow convection sub-grid scheme. The MKF stemmed from the original KF scheme and introduced new functions, such as resolution-dependent that adapt to the time scale of the convective process. (3) The NoCU represents the CUs that are not used, which also achieves good results at the "gray zone" grid spacing (~4–10 km resolution) (Ou et al. [53]; Qian et al. [106]).

For the PBLs, the Mellor-Yamada-Nakanishi-Niino (MYNN) Levels 2.5 (MYNN2.5) (Nakanishi et al. [110]) and the Yonsei University schemes (YSU) (Hong et al. [111]) are examined here. MYNN2.5 is tested by the Polar Meteorology Group, which is outstanding for polar environmental features and orographic influences (e.g., Xue et al. [65]; Bromwich et al. [67]; Hines et al. [78,79]). Moreover, the improvement of the reduction in the downward shortwave radiation bias has been verified as a significant improvement of Polar WRF V 4.1.1 (Xue et al. [65]; Olson et al. [112]). For the TP, YSU also has been frequently used (Ou et al. [53]; Gao et al. [97]; Chen et al. [104]; Gao et al. [105]; Qian et al. [106]). More importantly, when the MKF scheme is selected for CUs, the PBLs matched with YSU; that is, only the combination of MKF +YSU can be used in the model right now (Skamarock et al [81])

MPs dealing with cloud and precipitation particles must be parameterized in the numerical weather and climate models. The parameterizing of microphysics remains highly challenging because of the complexity of the underlying physics and the lack of understanding of these coupling processes (Bauer et al. [113]; Benjamin et al. [114]; Randall et al. [115]). Hence, a reasonable selection and modification of MPs are expected to achieve better simulation results of clouds and precipitation. Here, MPs are studied based on the research advances that have been extensively tested in the Arctic, Antarctica, and TP (Gao et al. [48]; You et al. [49]; Xue et al. [65,66]; Bromwich et al. [68]; Hines et al. [78]; Hines and Bromwich [80]; Gao et al. [97]; Qian et al. [106]; Zhu et al. [116]; Li et al. [117]; Ma et al. [118]; Shen et al. [119]; Yang et al. [120]; Zhang et al. [121]). Modify the liquid water droplet concentration in Morrison 2-mom to 50 cm⁻³ which has been verified to significantly improve the performance of polar clouds such as supercooled water in clouds (Xue et al. [66]; Hines et al. [78]; Hines and Bromwich [80]). TP, similar to the Antarctic and Arctic, is a colder region, and the liquid water of clouds more easily exists in the form of supercooled water. For the TP, the Morrison 2-mom specified droplet concentration of 100 cm⁻³ (referred to as M100) because of a greater amount of could particles (probably twice for maximum) and more prone to supercooled water than the Arctic (Yan et al. [122]). P3 (Morrison et al. [123]) used a new approach to predict the transformation of ice particles, named "one ice category," which represents a combination of ice, snow, and possibly graupel. The setting of double-moment for rain, ice, and cloud water and supersaturation-dependent activation is applied in this study (P51). Thompson aerosol-aware (Thompson et al. [124]) has been modified for mid-latitude convective, orographic, and snowfall conditions and considers water- and ice-friendly aerosols. WRF Double-Moment 6-class scheme is the double moment for warm-rain, and other processes are basically

Table 1. Summary of the characteristics of each experiment.

| Categories | Experiment | Description | Quantity | | | |
|--------------------------------------|------------------|---|----------|--|--|--|
| | Spectral nudging | The wave number17, 7. | | | | |
| Nudging | Grid nudging | Turn on / off nudging q . Nudging q coefficients is $0.0001/0.0002/0.0003$, respectively. | | | | |
| Cumulus parameterization (CUs) | GD | Grell-Devenyi Ensemble Scheme, multiple cumulus schemes and variants running within each grid box. The results are averaged with typically 144 subgrid members. | | | | |
| | G3 | Grell-3 Scheme, an improved version of the GD scheme, is more suitable for fine mesh grids (≤ ~10 km). Modified Kain-Fritsch Scheme, using the mass flux with downdrafts and CAPE removal time scale for deep and shallow convection sub-grid scheme. | | | | |
| | KF | | | | | |
| | MKF | Compared with the KF scheme, Multi-Scale Kain-Fritsch Scheme, due to the introduction of new functions such as resolution-dependent parameters, has the function of adapting to the time scale of the convective process. | | | | |
| | NoCU | Without cumulus parameterization. | | | | |
| Planetary boundary layer (PBLs) | MYNN2.5 | Mellor-Yamada-Nakanishi-Niino (MYNN) Levels 2.5, the local TKE (Turbulent Kinetic Energy) scheme is suitable for the stable environment at complex terrain in the polar region. The Yonsei University PBL, a revised vertical diffusion package with a nonlocal turbulent mixing coefficient, is an explicit treatment of entrainment processes at the top of the PBL. The MKF can only be combined with YSU this model version. | | | | |
| | YSU | | | | | |
| Microphysics (MPs) | M100** | Morrison double-moment scheme, good performance in the polar region. The default value of the droplet concentration is reduced to 100 cm ⁻³ in this study. Hydrometeor: five species including cloud droplets, cloud ice, rain, snow, and graupel/hail. Ice-Phase Processes: Yes Mixed-Phase Processes: Yes | | | | |
| | P51** | Predicted Particle Property scheme, one ice category that represents a combination of ice, snow and graupel, using the double moment rain, ice and cloud water setting | | | | |
| | TPA** | Thompson aerosol-aware, water- and ice-friendly aerosols. Hydrometeor: 5 species including cloud water, cloud ice, rain, snow, and | | | | |
| | WDM6** | | | | | |
| | WSM5* | | | | | |
| | WSM6* | WRF Single-Moment 6-class scheme, added graupel based on WSM5, suitable for high-resolution simulations. Hydrometeor: 5 species including water vapor, cloud, rain, ice, snow, and graupel. Ice-Phase Processes: Yes Mixed-Phase Processes: No | | | | |

^{**} double-moment, *sigle-moment

the same as WRF Single-Moment 6-class scheme (WSM6) (Lim et al. [125]). The condensation nuclei (CNN), such as cloud water and rain, adopt the "prediction method." It

performs reasonably well for high-resolution simulation studies in China (Zhu et al. $^{[116]}$; Li et al. $^{[117]}$; Shen et al. $^{[119]}$; Zhang et al. $^{[121]}$). Compared with the two-moment

schemes, single-moment schemes such as WRF Single-Moment 5-class scheme(WSM5) and WSM6 are often used as they can maintain a good balance between model skills and computational resources. And the WSM6 is also used and tested by the GRAPES_Meso operational weather forecasting model (Shen et al. [119]; Zhang et al. [121]; Huang et al. [126]; Ma et al. [127]). Table 1 shows a summary of the microphysics mentioned above, the hydrometeors, and whether ice-phase/mixed-phase processes are also included.

3.2 Validation data and methods

Considering the limited performance of observation and reanalysis over TP, multiple datasets are used to evaluate the simulations. The in situ observation obtains the daily precipitation dataset located in the TP and surrounding areas supplied by the TPDC (1979-2015, about 184 stations Fig. 1) (China Meteorological Data Network [128]). Satellite precipitation estimation products used the Tropical Rainfall Measuring Mission (TRMM) 3B42 V7 dataset with 3-hourly and $0.25^{\circ} \times 0.25^{\circ}$ resolution (Huffman et al. [129]). CRA-RA/Land, the first generation global atmosphere and land reanalysis released by the China Meteorological Administration. Probably assimilation of various conventional and satellite observations over East Asia, CRA-RA/Land is in good agreement with and even outperforms other reanalyses such as ERA5 datasets in near-surface variables over China (Li et al. [130]; Shen et al. [131]; Yang et al. [132]; Yu et al. [133]; Zhang et al. [134]). Precipitation estimates from CRA-Land with a horizontal resolution of ~34 km and a 6hour temporal interval. The ERA-Interim precipitation has been investigated as a benchmark and is also used in this study. The data is provided every 3 hours with a horizontal resolution of 0.75°×0.75°.

Due to the different spatial resolutions, the grid data are extracted and horizontally interpolated onto the domain by the WRF Preprocessing System (WPS) (e.g., Xue et al. [65]; Bromwich et al. [67]) with the same re-grid method. It is beneficial for comparisons using the same resolution (10 km) and grid points through the utilization of bilinear interpolation to interpolate grid data to station locations when comparing data between grid and in situ.

4. RESULTS

4.1 Impacts of model options for precipitation

In this section, the multiple aspects of the model option for precipitation over the TP nearby areas are examined by the sensitivity experiments. Considering the main targets of this study and successor work, the variations of monthly and daily precipitation between multiple model settings are evaluated against in situ, satellite observations, and reanalyses. It focuses on the spatiotemporal comparison of large-scale and average conditions and does not analyze the specific rainfall processes, such as comparing rainfall forecasts by the Threat Scores (Jiang et al. [135]; Mesinger [136]; Yang and Tung [137]). Here, January and July, the two months with the largest difference in a year are used to investigate. Since the precipitation is mainly occupied in the summertime, the analysis of the precipitation characteristics of each experiment in July 2015 is discussed below.

4.1.1 NUDGING

Figure 2 shows the results of precipitation in July 2015 under different nudging settings and the references with ERA-Interim (EI), CRA-Land (CRA), and TRMM 3B42 (TRMM), respectively. Overall, the model well

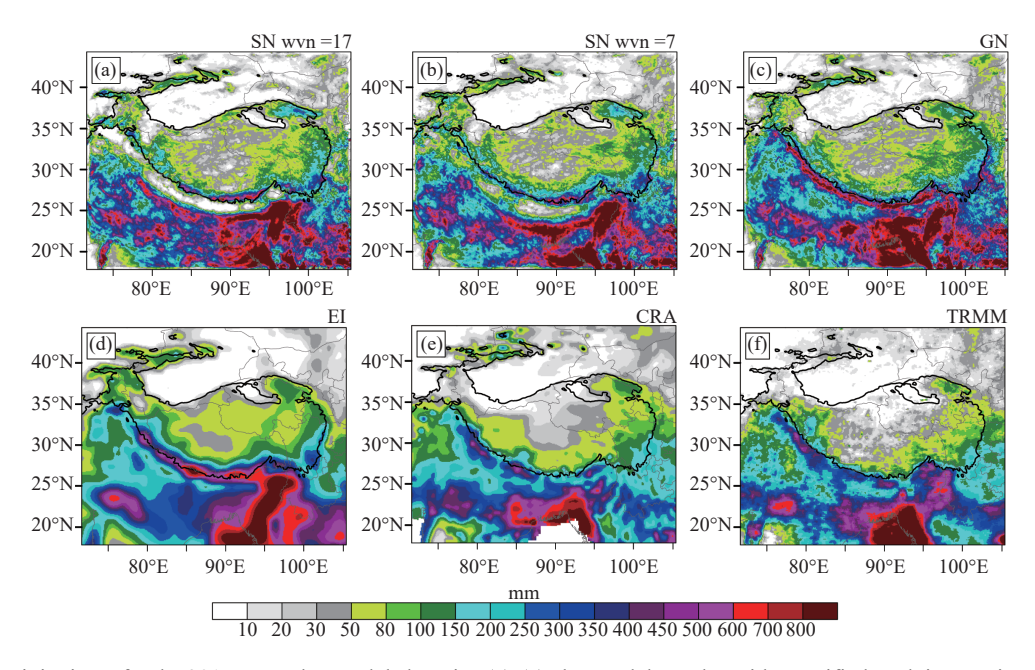


Figure 2. Precipitation of July 2015 over the model domain. (a)-(c) the model results with specified nudging settings. (a) Spectral nudging wave number was specified as 17, (b) the wave number was specified as 7, and (c) grid nudging; (d)-(f) ERA-Interim (EI), CRA-Land (CRA), TRMM 3B42 (TRMM). The black solid line indicates the altitude of 3000 m.

captures the main characteristics of precipitation distribution over the domain. Precipitation decreases from southeast to northwest, and there is a clear borderline along the edge of the plateau (such as an altitude of 3000 m). The Bay of Bengal has the most precipitation amount, with a maximum value of more than 800 mm, whereas the Tarim Basin is the region with the least, with most areas less than 10 mm. At the same time, it can also be seen that EI has the largest precipitation, with most areas on the plateau having more than 50 mm during this month. CRA and TRMM are roughly similar, and the covering of precipitation greater than 50mm is significantly smaller than EI. For TRMM, we also noticed that the precipitation in the northern part of the domain (north of 35°N, such as the Tianshan area) is insufficient. It is likely to be related to the low coverage of TRMM data in extratropical regions.

Further analysis shows that the results of spectral nudging (Fig. 2 (a) and (b)) located a very weak anomalous precipitation belt along the southern side of the Himalayas. This belt is also accompanied by an abnormally strong surface short-wave down and weak long-wave radiation (not shown), which indicates that the low cloud cover and the convective process might be restricted. In addition, the tests also found that the intensity of this abnormal precipitation belt is related to the wave number used. For instance, when the wavenumbers are selected as 17, 7, and 3 (the cutoff wavelength is roughly equal to ~350 km, ~800 km, and ~1800 km, respectively), the belt gradually blurred with the wavenumber decreases.

In other words, the model has more freedom as the wave number decreases, and the impacts of nudging on medium scales are also weakened. That means the modulation for overestimation precipitation is suppressed. The grid nudging result is different from spectral nudging, which is consistent with EI, CRA, and TRMM maintaining a strong precipitation belt on the south side of the Himalayas. Some possible reasons can be inferred as follows. The spectral nudging skills are determined by the nudge scale, which is related to the model domain and the scale of driving fields (Skamarock et al. [81]; Liu et al. [101]; Miguez-Macho et al. [138]). The southern foothills of the Himalayas are more sensitive to scale due to the complex local topographical and convective variations. Thus, the skill of spectral nudging really penalizes here. However, the option of grid nudging can avoid "scale selection" and good performance with precipitation and moisture adjustment (e.g., Bowden et al. [139]; Wootten et al. [140]). Therefore, it shows better performance.

Nudging toward the water vapor mixing ratio is believed to be beneficial for the simulation of precipitation and moisture (e.g., Mai et al. [141]; Spero et al. [142]). Therefore, the impacts of nudge q and its strength are examined. First of all, sensitive test results indicate nudging q can significantly improve precipitation on the plateau. In the central and northern parts of the plateau, where precipitation is overestimated (such as exceeding 50 mm), there is a significant decrease (not shown). More details are shown in Fig. 3. It gives the difference in monthly precipitation between model results with specified

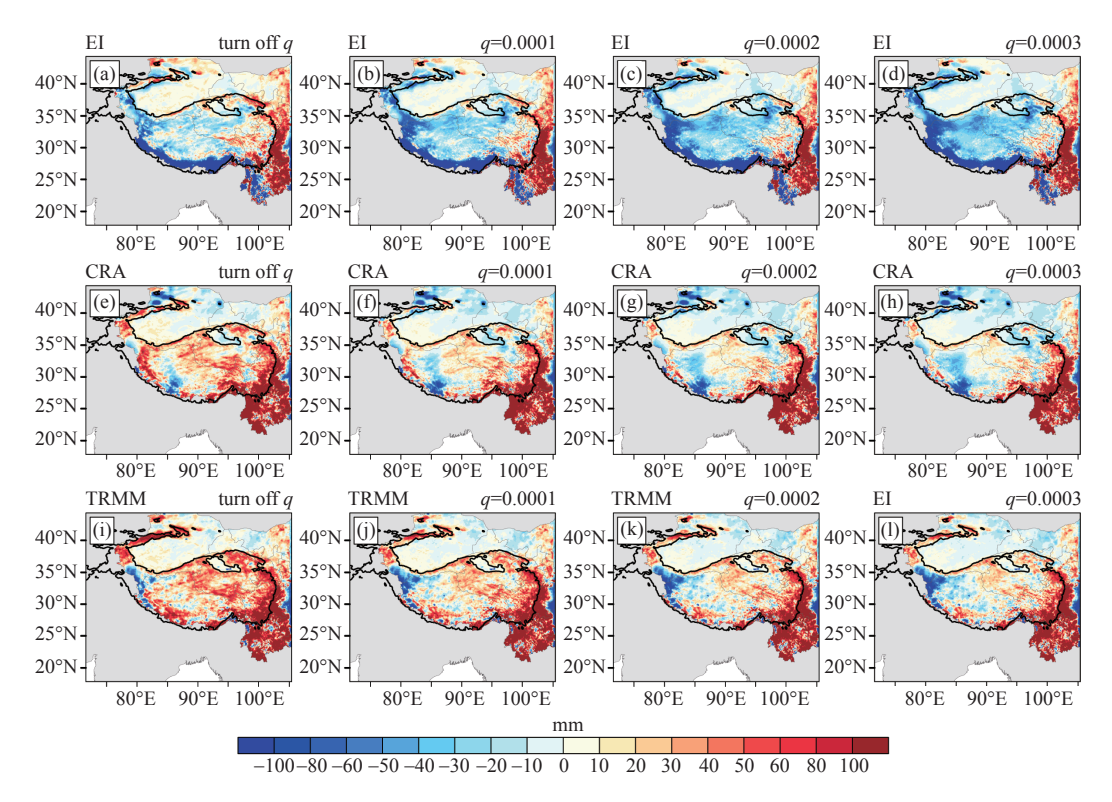


Figure 3. Precipitation difference in July 2015 with specified grid nudging settings. Model minus ERA-Interim (EI), CRA-Land (CRA), TRMM 3B42 (TRMM), respectively. The columns from left to right are turned off nudging q, nudging q coefficients as 0.0001, 0.0002 and 0.0003, respectively. The black solid line indicates the altitude of 3000 m.

grid nudging settings and EI, CRA, and TRMM, respectively. Although the simulation precipitation minus each dataset shows more variation, it is consistent that the superfluous precipitation can be reduced by nudging q, and the greater the intensity of the nudging coefficient, the more significant the effect on the reduction of precipitation. Compared with EI, the model mainly shows a negative difference, especially along the western and southern mountain margins, where there is a precipitation belt with negative 80-100 mm. This is probably caused by the overestimation of precipitation over these areas from EI. Both the differences in the model minus CAR and TRMM indicate the negative values in the west while positive in the central and eastern parts of the plateau. The maximum positive region is located at the east edge of the plateau and the Hengduan Mountains. It is consistent with the general inability of current models to simulate precipitation in this region (Chen et al. [45]). It is worth noting that with increasing the intensity coefficient of nudging q, the positive trend on the central and eastern TP will decrease, and the changes are intensifying correspondingly in the western plateau. Thence, tradeoffs for the obvious regional features possessed by nudging q. The intensity coefficient is 0.0002 for q and other settings, including nudging u, v, t, and ph, using the same value of 0.0003. All the nudging applied above the vertical 35 layers higher than the top of the PBL reasonably improved the model performance at the upper layers (Xue et al. [65]; Mai et al. [141]).

4.1.2 CUMULUS PARAMETERIZATION

Since EI significantly overestimates precipitation in the southern TP and TRMM underestimates in the north, Fig. 4 only shows the monthly precipitation difference of the model minus CRA for July 2015. At present, MKF can only be combined with YSU. Therefore, the suite of cumulus with MYNN2.5 and YSU are tested, respectively. It is clear that the model simulated with CUs usually produced too much precipitation, but NoCUs seems precipitation is not enough conversely. Furthermore, the impacts of different CUs on precipitation are also evident. Fig. 4a-c shows that G3 has the most significant positive difference in precipitation, and KF produces too much precipitation covering large areas such as the east and south of TP (the Hengduan Mountains). We also noticed that the G3 scheme produced more precipitation than GD (Fig. 4b-c), which had been investigated by the simulation analysis of the precipitation over the southern slopes of the TP (Wu et al. [56]). The MKF performed much superior to KF (Fig. 4d-e). It means the scale adaptive cumulus scheme shows better skills for precipitation over the TP. In other words, it is that making use of scale-aware performs superior for solving interaction/uncertainty problems, especially for simulations forced by complex terrain and low confidence in initial and lateral boundary conditions. Therefore, MKF is suggested for priority use.

4.1.3 PLANETARY BOUNDARY LAYER

Figure 4 also remarkably indicates that GD +MYNN2.5 and MKF+YSU are better at simulating precipitation. And MKF+YSU seems more sophisticated as over the eastern side of the TP (such as west of Sichuan Basin), the central part (the Three-River headwater region), and northern India (figure omitted), the precipitation performed by GD+MYNN2.5 more superfluous than that of MKF+YSU. Due to the different setting suites, KF+YSU and KF+MYNN2.5 served as supplementary to determine MKF and YSU, which one improved model skills more significantly. Compared with MKF+YSU (Fig. 4d), KF+YSU (Fig. 4e) overestimated precipitation at central and eastern TP. It indicates that MKF has better performance than KF. Correspondingly,

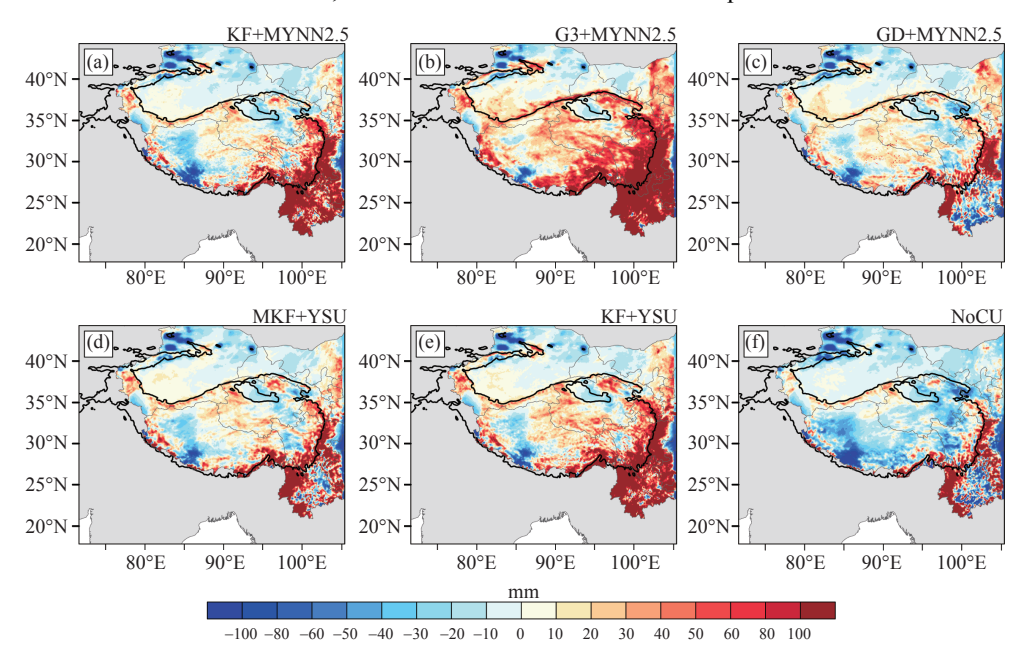


Figure 4. Precipitation difference in July 2015 from the model with specified CUs and PBLs. Model minus CRA-Land. The black solid line indicates the altitude of 3000 m.

the results of KF+MYNN2.5 (Fig. 4a) and KF+YSU (Fig. 4e) revealed that MYNN 2.5 shows the ability to improve precipitation slightly compared to TP. However, as the MKF performs greater modeling skills, the MKF+YSU performs much better. In other words, compared with MKF, both YSU and MYNN2.5 could have a limited impact on precipitation simulation.

4.1.4 MICROPHYSICS

Based on the optimized settings for nudging, CUs, and PBL, microphysics options can be further examined to expand the knowledge for a "better-performing" configuration suite. Fig. 5 compares the spatial distribution of the precipitation difference from the model with specified microphysics minus CRA. Significant differences indicate that the model configured with different microphysics offers a wide variety of capabilities or limitations. Among the four doublemoment schemes, M100, P51, and TPA carried similar results. Compared with CRA, precipitation is overestimated in the eastern slope of TP (such as the western Sichuan Basin), the southern foot of the Nyaingentanglha Mountains, and the western slope of the Hengduan Mountains, etc. On the contrary, in the Tianshan Mountains and other places in the west of the TP (west of ~85°E), the modeling precipitation is less than that of the CRA. Specifically, M100 is close to P51. However, the negative values of M100 in the west of the plateau are smaller, and it is much closer to CRA. TPA is slightly poor, and too much precipitation is produced in the southeast, such as Yunnan and Guizhou. For WDM6, it is evident precipitation is underestimated in the east of TP while slightly overestimated in places such as the Kunlun Mountains in the northwest of TP. In the two singlemoment schemes, WSM5 is similar to WDM6 but with significantly less precipitation. WSM6, which extended

the WSM5 by adding additional processes related to graupel (Hong ^[143]), performs much better than WSM5 and is roughly comparable to M100 and P51.

To evaluate the finer differences, the RMSE (Root Mean Square Error) and precipitation difference from model data against in situ observations were calculated. Fig. 6 shows the RMSE value and spatial distribution from the model with specified MPs accompanied by EI, CRA, and TRMM that are used as references. First, RMSE exhibits increasing from the northwest (values are usually less than 4 mm) to the southeast (most are greater than 10 mm). In particular, the maximum RMSE is mainly distributed in the Hengduan Mountains and on the edge of the Himalayas. One aspect is likely related to the higher absolute precipitation that produces larger biases. On the other hand, it is still challenging for the model to simulate precipitation under the complex terrain and strong water vapor transport conditions over the TP and surroundings. Compared with different MPs, M100 and WDM6 show less RMSE than the other two double-moment schemes at the southeast of TP. The single-moment schemes indicate a similar spatial pattern to that of double-moment schemes, and WSM5 shows less RMSE than WSM6. Furthermore, we analysed the differences in monthly precipitation. Although WDM6 and WSM6 perform better RMSE, precipitation is systematically underpredicted compared to in situ observation (Fig. 7), which is consistent with the previous findings compared with CRA (Fig. 5). By comparison with in situ dataset, Fig. 6 and Fig. 7 also verify that the CRA shows the best performance in the 3 kinds of grid precipitation products.

Considering the significant spatial variation of precipitation differences through the TP, the region is divided into four sub-regions along 34°N (Li [144]) and 95°E (Gao et al. [3]). That is, Northwest (NW), Northeast

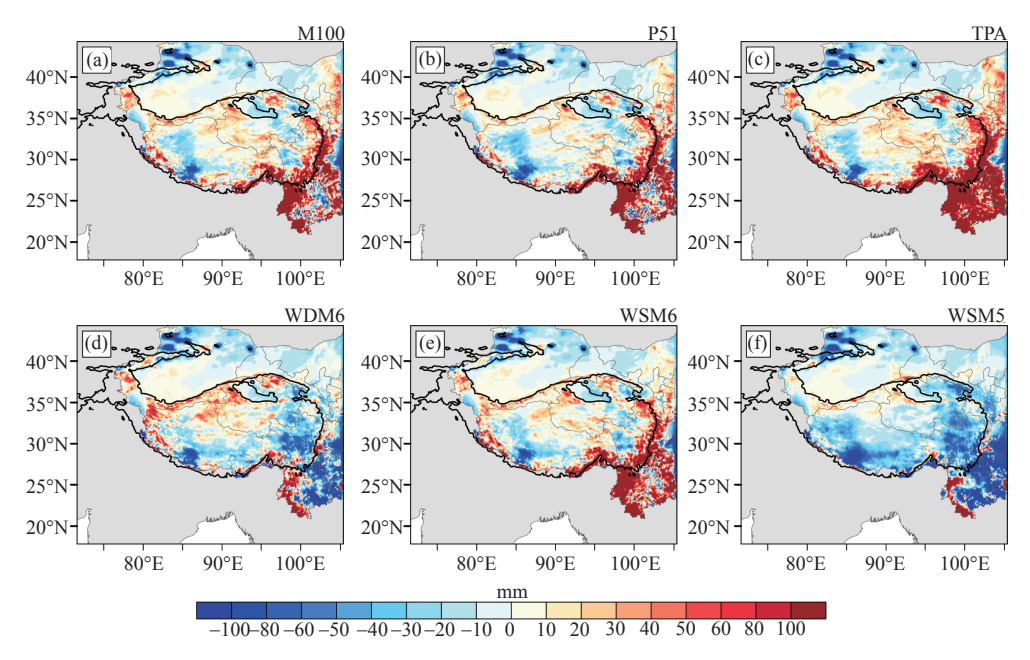


Figure 5. Precipitation difference in July 2015 from the model with specified MPs. Model minus CRA-Land. The black solid line indicates the altitude of 3000 m.

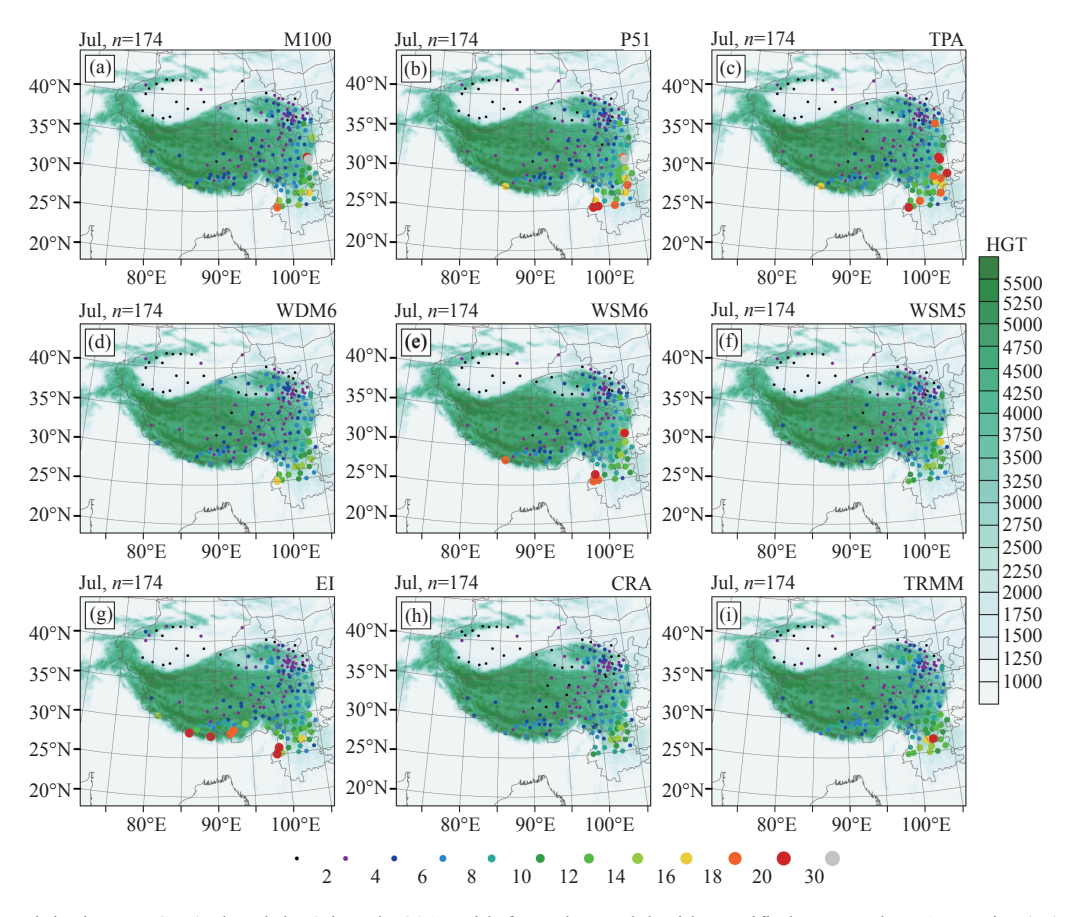


Figure 6. Precipitation RMSE (colored dots) in July 2015 with from the model with specified MPs and ERA-Interim (EI), CRA-Land (CRA), and TRMM 3B42 (TRMM), respectively. Model/Reanalysis minus in situ observation. The black solid line indicates the altitude of 3000 m.

(NE), Southeast (SE), and Southwest (SW), and the number of in situ stations in each sub-region are 24, 53, 68, and 29, respectively. Fig. 8 gives the whole TP and its sub-regions of station-averaged precipitation in July 2015 from the model with specified MPs. It can be seen that among the four sub-regions, the precipitation in the SE is the largest while the NW is the smallest, which is about one-tenth of SE. NE and SW are equivalent, probably half of the SE. These characteristics are consistent with the spatial distribution discussed above that the precipitation decreases from southeast to northwest over TP. The difference is mainly in the southern TP (south of 34°N), especially in the SE and SW, where MPs perform significant impacts on precipitation. For instance, in SE where is the most significant precipitation difference, the maximum (TPA 201 mm) is more than 2.5 times larger than the minimum (WSM5 77 mm). From Fig. 8, the overarching findings are that the M100, WSM6, P51, and TPA are relatively overestimated precipitation, whereas WSM5 and WDM6 are underestimated precipitation. It also can be seen that M100 is superior to others and is closest to CRA and in situ observation, respectively.

4.2 Performance of precipitation simulation

Standing on the "better-performing" configuration investigated above, the performance of precipitation simulation using Polar WRF can be confidently further

discussed in the following sections. The refined model parametrizations are as follows: grid nudging is used, where the q intensity coefficient is 0.0002 while the rest are 0.0003; the MKF cumulus parameter scheme; the YUS boundary layer parameter scheme and the M100 as the microphysics. Here, as mentioned in the introduction, a full calendar year simulation and compared with multiple reanalyses and observations are carried out.

4.2.1 BASIC CHARACTERISTICS OF ANNUAL PRECIPITATION

Figure 9 shows the annual precipitation over TP and the surrounding regions from simulation, EI, CRA, TRMM, and in situ observations. All the results show an evident similar pattern in that precipitation decreases from southeast to northwest, as discussed above. Further comparison with station observations, EI exhibits more precipitation over the domain while TRMM does not have enough precipitation north of ~35°N. For CRA, most areas are very close to the observation except for some stations on the edge of 3000 m of the southeast. Although the precipitation on the western slope of the Hengduan Mountains and the eastern slope of TP is relatively heavy, the distribution of M100 performs consistently with observations. By examining the annual precipitation frequency, the abnormally high frequency of precipitation can be seen in the EI, CRA, and M100. But M100 shows much better performance than the two

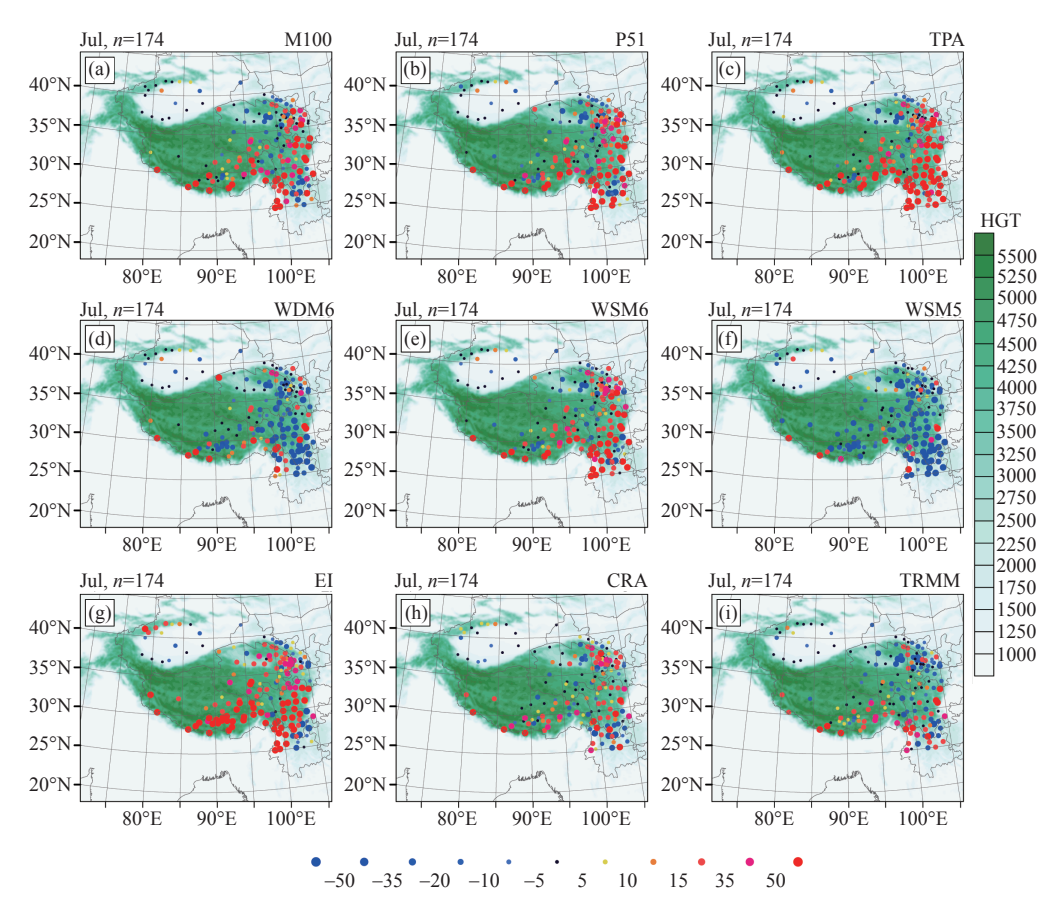


Figure 7. Precipitation difference (colored dots) in July 2015 from the model with specified MPs and ERA-Interim (EI), CRA-Land (CRA), and TRMM 3B42 (TRMM), respectively. Model/Reanalysis minus in situ observation. The black solid line indicates the altitude of 3000 m.

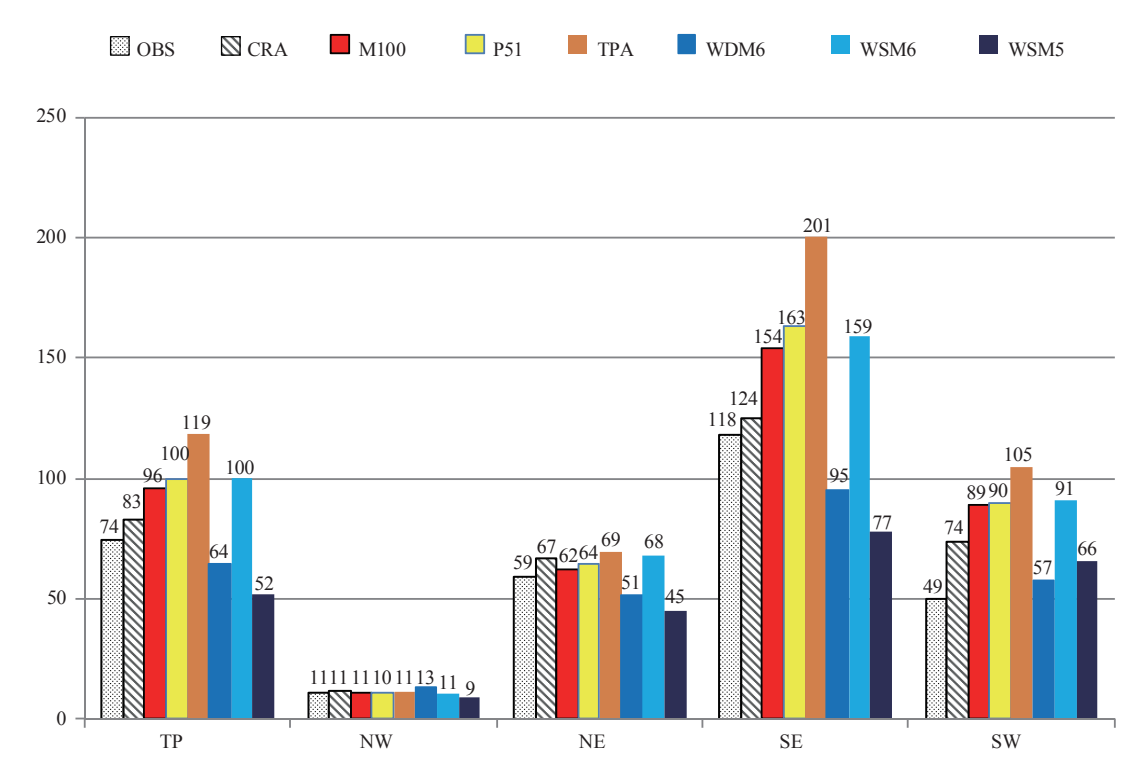


Figure 8. Station-averaged precipitation in July 2015 from the model with specified MPs, in situ observation (OBS), ERA-Interim (EI), CRA-Land (CRA) and TRMM 3B42 (TRMM), respectively (units: mm).

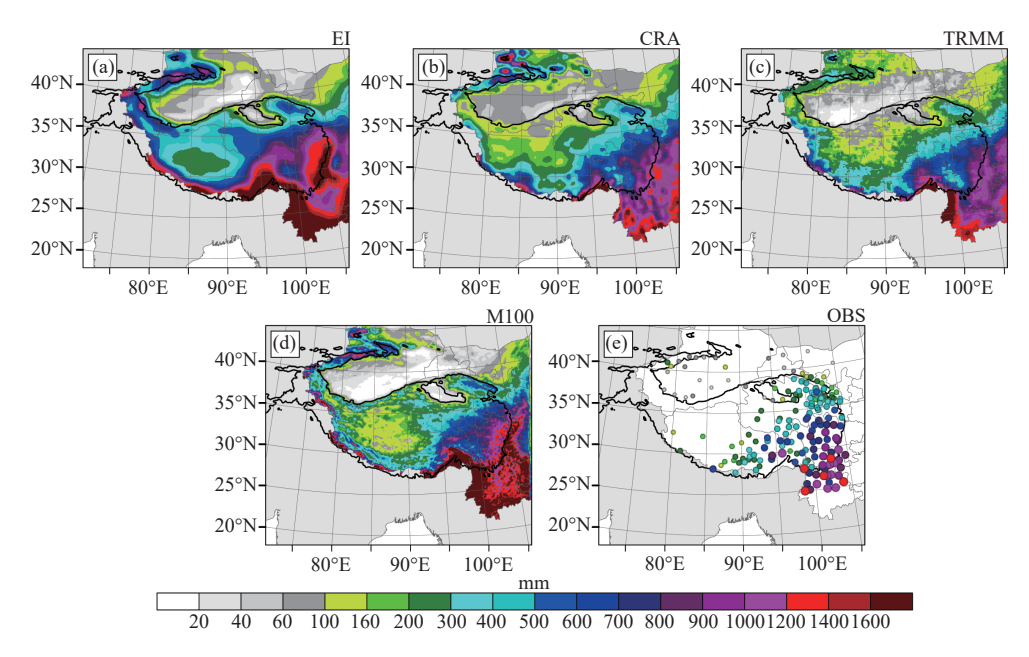


Figure 9. The distribution of annual precipitation over the Qinghai-Tibet Plateau and the surrounding regions. The black solid line indicates the altitude of 3000 m.

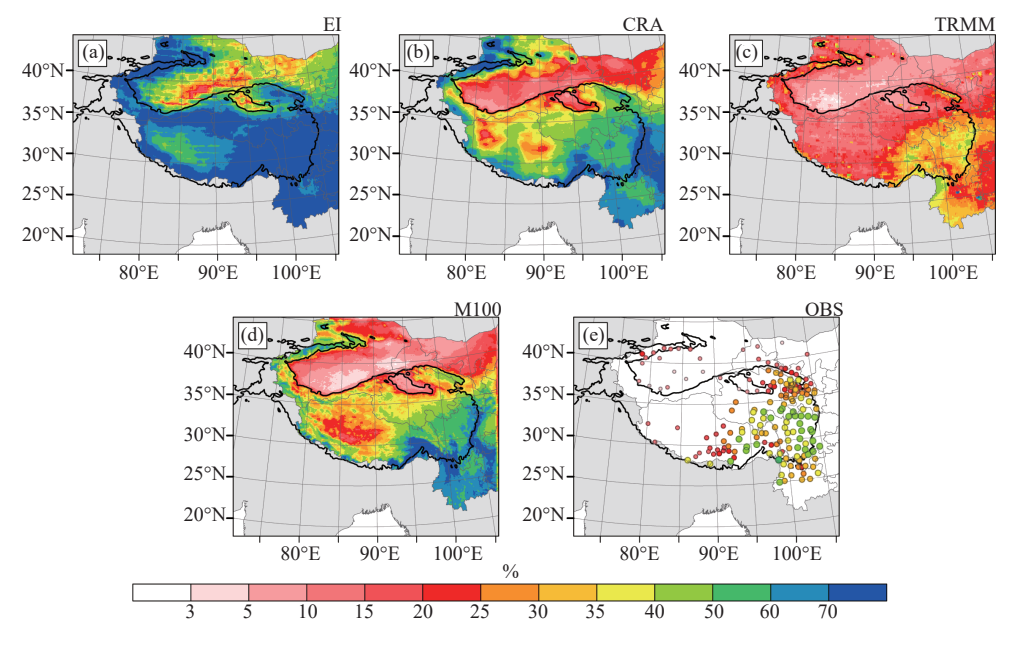


Figure 10. The distribution of annual precipitation frequency over the Qinghai-Tibet Plateau and the surrounding regions. The black solid line indicates the altitude of 3000 m.

reanalyses, such as the western slopes of the Hengduan Mountains, the eastern slopes of TP, and the Tianshan Mountains (Fig. 10). Corresponding to these features, the annual precipitation intensity from models and reanalyses is also weaker than observations. M100 presents superior to the two reanalysis data, especially in the southeast of TP (Fig. 11).

4.2.2 MONTHLY AND DAILY PRECIPITATION

Monthly and daily precipitation can describe more spatial and temporal variations and have been used to examine precipitation performance (e.g., Bai et al. ^[61]; Li et al. ^[130]; Jeworrek et al. ^[145]). Fig. 12 shows monthly station-averaged precipitation, including the whole TP and

its sub-regions from January to December 2015. Precipitation has significant annual temporal variation and regional spatial characteristics. The precipitation is mainly concentrated in the summer half year. The amounts from May to September account for 70%–80% of the annual precipitation. Among them, in situ observation (OBS) is 80.0%, M100 is 74.4%, EI is 72.2%, CRA is 79.5%, and TRMM is 80.3%. Moreover, the precipitation from April to October contributed more than 90% of the annual precipitation (only EI accounted for 87.4%, and the rest ranged from 90.2% to 92.9%). This intra-annual variability is in step with the outbreak, maintenance, and retreat of the Asian summer monsoon.

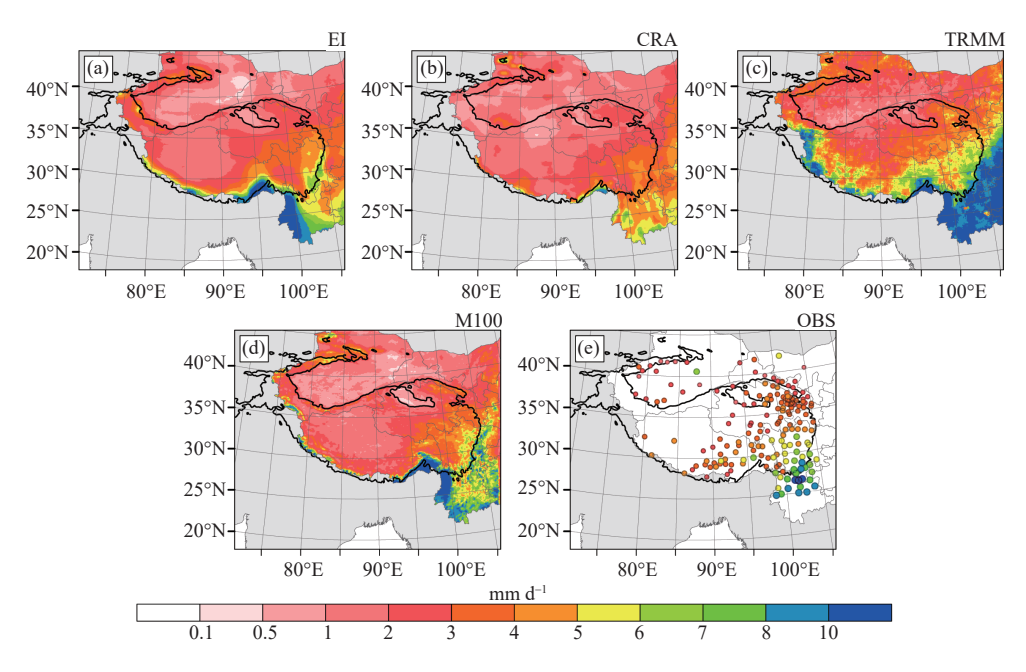


Figure 11. The distribution of annual precipitation intensity over the Qinghai-Tibet Plateau and the surrounding regions. The black solid line indicates the altitude of 3000 m.

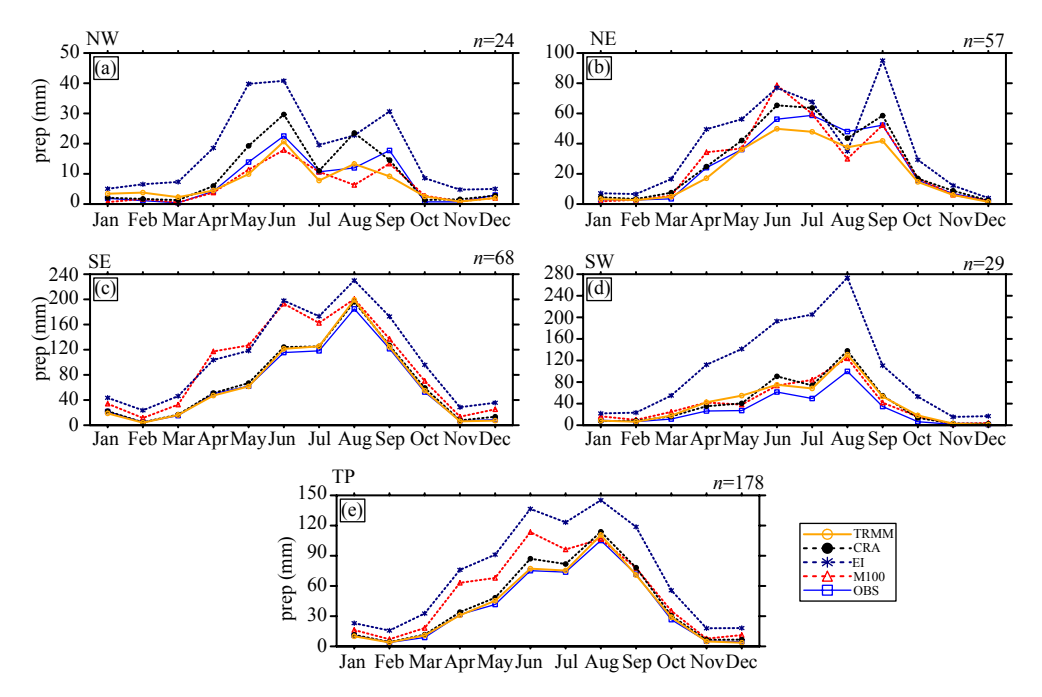


Figure 12. Monthly station-averaged precipitation from January to December in 2015. (a) NW, 24 stations; (b) NE, 57 stations; (c) SE 68, stations; (d) SW, 29 stations; (e) TP, 178 stations.

For the three precipitation products, CRA and TRMM are relatively close to those observed by the station, and CRA is slightly larger. The precipitation from TRMM in the northern TP (NW, NE) is somewhat underestimated, whereas that in the southern TP (SE, SW) is slightly overestimated. This is also the reason why TRMM has the smallest statistical precipitation difference between the whole TP and station observations. Obviously, EI shows too much precipitation, especially in the sub-regions of SE and SW. Two reasons might be related to this. One, EI has relatively large precipitation in these areas, so the ability to represent precipitation in complex terrain areas such as the

south is limited. The two horizontal resolution of EI is the lowest in the four grid data used here; it may produce larger errors than others after interpolation.

The model's monthly precipitation is evidently better than EI and generally close to CRA and TRMM, even particularly slightly superior to CRA and TRMM in the NW and SW sub-regions. However, over the SE, the monthly precipitation trend is quite well depicted by the model, but the simulated precipitation is still too overestimated. This is probably due to the sparse observations and the limited direct observation data available for data assimilation at the NW and SW. CRA

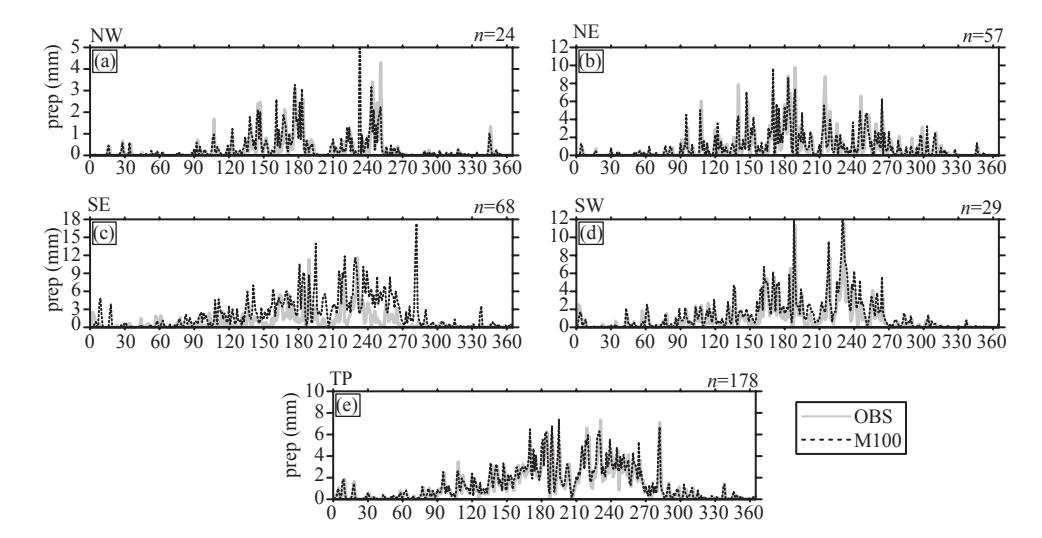


Figure 13. The time series of daily station-averaged precipitation in 2015. The grey solid line and black dashed line indicate observation and model output, respectively. (a) NW, 24 stations; (b) NE, 57 stations; (c) SE, 68 stations; (d) SW, 29 stations; (e) TP, 178 stations.

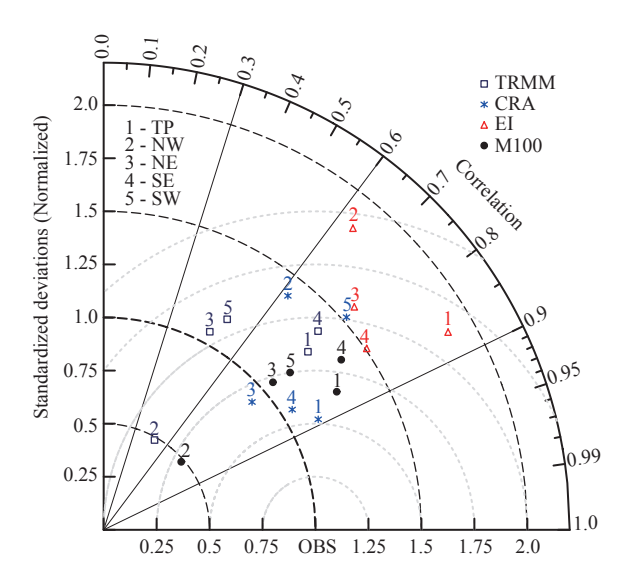


Figure 14. Daily precipitation of Taylor diagram for Model (M100), ERA-Interim (EI), CRA-Land (CRA) and TRMM precipitation (TRMM) compared with what was observed in 2015. The direction of the azimuth cosine is the correlation, the distance to the azimuth is the normalized variance ratio, and the distance to the reference point (OBS) represents the RMSE of the observation. The poor results of EI in the SW area are not shown in the figure; that is, only 4 values are displayed.

failed to show a better advantage, while the downscaling of the model has certain advantages. In particular, the model optimizes the ice-snow-atmosphere interaction and performs better in the area with large ice and snow coverage in the west of TP. On the contrary, observations in the eastern region are relatively abundant, and CRA performs better in this region as richer observations have been assimilated (Li et al. [5]; Li et al. [130]). In addition, since the initial and lateral boundary conditions derived from EI, it will also lead to large positive abnormalities where precipitation is overestimated dramatically, such as in the southeast of TP. These findings also suggest the importance of data assimilation (improvement of initial

Table 2. The correlation, bias and RMSE of M100 and CARLAND against in situ observation for daily precipitation.

| | | TP | NW | SW | NE | SE |
|------|------|------------|------------|------------|------------|------------|
| CORR | M100 | 0.86 | 0.75* | 0.76* | 0.75 | 0.81 |
| | CRA | 0.89^{*} | 0.62 | 0.75 | 0.76^{*} | 0.84^{*} |
| Bias | M100 | 0.44 | -0.05^* | 0.39^{*} | 0.05^{*} | 0.99 |
| | CRA | 0.15^{*} | 0.07 | 0.41 | 0.09 | 0.14 |
| RMSE | M100 | 0.95 | 0.37^{*} | 1.15* | 1.10 | 2.08 |
| | CRA | 0.73^{*} | 0.54 | 1.30 | 1.06* | 1.52* |

^{*} Indicates the better one

conditions) and model-driving data for the regional model.

Unifying the mode results in the daily temporal resolution as the in situ, Fig. 13 displays the time series of daily station-averaged precipitation in 2015. The model shows an excellent ability to capture the daily precipitation evolution during the annual cycle. It skillfully describes the precipitation characteristics over TP and nearby areas. In the view of temporal distribution, precipitation is mainly produced from April to October (90-300 days on the X-axis in Fig. 13), which is consistent with the above finding. The daily precipitation also shows good agreement between the model and observations. The disadvantage is that the peak of daily precipitation simulated by the model is smaller than the observation. It indicates that the model is limited in simulating some heavy/extreme precipitation, which also caused the shortcoming of weak intensity for precipitation mentioned in 4.2.1. In addition, it can also be seen clearly that the daily precipitation in the SE from April to July (90–210 days on the X-axis in Fig. 13) is greater than the observation. Which further verifies the results discussed above.

To combine multiple data into a comprehensive evaluation, Fig. 14 shows the daily precipitation of the Taylor diagram for M100, CRA, and TRMM, respectively. The daily precipitation simulated by the model (black dot)

is at the forefront among the results, and the correlation of each region is in the range of 0.75–0.86 (Table 2). which is better than others. Also, the distribution of each region exhibited in the figure is relatively concentrated, which indicates the model skills in various regions of TP are relatively stable. In general, the model performance is comparable to that of CRA, especially in the NW and SW, which is better than the former. This is also supported by a quantitative comparison of the correlation, bias, and RMSE that are shown in Table 2. Although the monthly precipitation from TRMM is the closest to the observation, the analysis of daily precipitation shows that it is not superior to others. The results generally show a smaller correlation and larger RMSE (the blue box in Fig. 14). This suggests that TRMM is limited for characterizing the evolution of the refined precipitation. EI (the red triangle in Fig. 14) performs worst, and the ability to describe the daily precipitation is extremely limited. Moreover, the distribution of each point is too widespread to draw the SW whose results are beyond the scope of the illustration

5. CONCLUSION AND DISCUSSION

Considering it is still facing challenges for numerical models and reanalysis to describe the precipitation over the TP and its surrounding region, this study extended the testing and applied the Polar WRF model to expand the knowledge of modeling precipitation.

Firstly, based on the model ground surface properties upgrade and the optimized Noah-MP, the impacts of nudging, CUs, PBLs, and MPs on summer precipitation are comprehensively examined by 4 categories of 19 groups of sensitive experiments with the 10 km horizontal resolution. The "better-performing" options suite is as follows.

- (1) Nudging helps to quantify forecasting and modeling uncertainties. The spectral nudging skills are determined by the nudge scale which is more sensitive to the complex local topographical and convective variations over the TP and nearby areas. The option of grid nudging can avoid "scale selection" and good performance with precipitation and moisture adjustment. That is, grid nudging is suggested. By trade-offs, keep the balance of model "drift" and "freedom," the intensity coefficient is 0.0002 for q and other settings, including nudging u, v, t, and ph using the common values of 0.0003.
- (2) For CUs, the MKF is suggested for priority use because the scale-aware scheme performs superior in solving interaction/uncertainty for simulations forced by complex terrain and low confidence in initial and lateral boundary conditions. The ensemble scheme displayed the more complex situation. GD and G3 show different simulation skills, and GD is much better. However, due to the limited work here, further research is absolutely needed to verify why the G3 scheme causes significantly more precipitation on the east side of the TP.
- (3) Compared with the CUs, both YSU and MYNN2.5 could have a limited impact on precipitation

simulation. Although MYNN 2.5 also shows the ability to improve precipitation. However, because only the combination of MKF+YSU can be used in the model right now, YSU is selected for PBLs at the end.

(4) A wide variety of capabilities or limitations are shown in MPs' options. The overarching findings are that the M100, WSM6, P51, and TPA are relatively overestimated precipitation, whereas WSM5 and WDM6 are underestimated precipitation. It also can be verified that M100 performs more reasonably than others and is closest to CRA and in situ observation, respectively.

Then, precipitation simulation for a full calendar year and compared with multiple reanalyses and observations are used for further evaluation. The downscaling simulations indicate that Polar WRF can successfully capture the general features over TP and performs more sophisticated than EI and TRMM. For the monthly and daily precipitation, it is equal to or even slightly better than CRA, especially in the western part of the plateau where the observations are sparse and the ice-snow-atmosphere interaction is more significant. In addition, It is worth noting that the performance of multiple precipitation products works quite differently over the TP and the surrounding regions. Overall, CRA is better than TRMM, and TRMM is superior to EI. Therefore, multi-sources of blended precipitation should be considered as a reference in the future.

This study also extends the findings of model defects. Although the model exhibits reasonable skills, it still underperforms in simulating precipitation under the complex terrain and strong water vapor transport conditions over the TP and the surroundings. The shortcomings include precipitation overestimation and precipitation with higher frequency and weaker intensity, which certainly need to be further improved. Furthermore, due to the key purpose of this study, only limited testing for the model based on knowledge of using Polar WRF and WRF model. More model option suites and refined evaluations are vet to be carried out, such as multi-vear simulations, higher convection-permitting resolution, and multiple physics ensembles. Also, the precipitation diurnal variation, the rainfall peak, and the duration of rainfall events should be taken into account in future work.

In addition, better-driving data should be further considered. As the higher vertical resolution driving data is beneficial for the Polar WRF model (Xue et al. ^[65]), the ERA-Interim 60 model levels reanalysis is employed to initialize and drive model runs. However, ERA-Interim has been verified to overestimate precipitation over the TP, especially in the sub-region of SE and SW. It also probably contributes to the overestimation of model precipitation in these regions, with the ERA-Interim being used as the global model field used for nudging.

To summarize, this study comprehensively investigates the impacts of multiple options. It provides valuable information about the simulation of precipitation across a variety of Polar WRF model metrics over the TP

and its surrounding regions. Despite the inevitable limitations studies entail, hopefully, our findings can help Polar WRF users and developers with their model configurations and better understand the model characteristics beyond the Antarctic and Arctic.

Acknowledgements: Thanks go to the Polar Meteorology Group at the Byrd Polar and Climate Research Center of Ohio State University provides the Polar WRF Model. In particular, we are grateful to Dr. David H. Bromwich and Lesheng Bai for their valuable suggestions for the Polar WRF model testing and application. We want to thank the National Tibetan Plateau/Third Pole Environment Data Center and China Meteorological Data Network for the observations and CRA data. We appreciate the use of TRMM 3B42 and ERA-Interim, which were downloaded from NASA and the ECMWF data servers, respectively. Thanks for the comments from the reviewers and editors that substantially improved this article.

REFERENCES

- [1] BIBI S, WANG L, LI X, et al. Climatic and associated cryospheric, biospheric, and hydrological changes on the Tibetan Plateau: a review [J/OL]. International Journal of Climatology, 2018, 38(S1): e1–e17, https://doi.org/10.1002/joc.5411
- [2] CHEN H, ZHU Q, PENG C, et al. The impacts of climate change and human activities on biogeochemical cycles on the Qinghai-Tibetan Plateau [J]. Global Change Biology, 2013, 19(10): 2940–2955, https://doi.org/10.1111/gcb.12277
- [3] GAO Y, XU J, CHEN D. Evaluation of WRF mesoscale climate simulations over the Tibetan Plateau during 1979– 2011[J]. Journal of Climate, 2015, 28(7): 2823–2841, https:// doi.org/10.1175/JCLI-D-14-00300.1
- [4] KANG S, XU Y, YOU Q, et al. Review of climate and cryospheric change in the Tibetan Plateau [J]. Environmental Research Letters, 2010, 5(1): 015101, https://doi.org/ 10.1088/1748-9326/5/1/015101
- [5] LI G, CHEN H, XU M, et al. Impacts of topographic complexity on modeling moisture transport and precipitation over the Tibetan Plateau in summer [J]. Advances in Atmospheric Sciences, 2022, 39(7): 1151–1166, https://doi. org/10.1007/s00376-022-1409-7
- [6] TONG K, SU F, YANG D, et al. Tibetan Plateau precipitation as depicted by gauge observations, reanalyses and satellite retrievals [J]. International Journal of Climatology, 2014, 34(2): 265–285, https://doi.org/10.1002/joc.3682
- [7] YANG M, WANG X, PANG G, et al. The Tibetan Plateau cryosphere: observations and model simulations for current status and recent changes [J]. Earth-Science Reviews, 2019, 190: 353–369, https://doi.org/10.1016/j.earscirev.2018.12.018
- [8] YAO T, XUE Y, CHEN D, et al. Recent Third Pole's rapid warming accompanies cryospheric melt and water cycle intensification and interactions between monsoon and environment: multidisciplinary approach with observations, modeling, and analysis [J]. Bulletin of the American Meteorological Society, 2019, 100(3): 423–444, https://doi. org/10.1175/BAMS-D-17-0057.1

- [9] YOU Q, WU T, SHEN L, et al. Review of snow cover variation over the Tibetan Plateau and its influence on the broad climate system [J]. Earth-Science Reviews, 2020, 201: 103043, https://doi.org/10.1016/j.earscirev.2019.103043
- [10] LI F, GAO Y Q, WAN X, et al. Earth's "three-poles" climate change under global warming [J]. Trans Atmos Sci, 2021, 44(1): 1–11, https://doi.org/10.13878/j.cnki.dqkxxb.20201031003, in Chinese with English abstract
- [11] SUN J, YANG K, GUO W, et al. Why has the Inner Tibetan Plateau become wetter since the mid-1990s? [J]. Journal of Climate, 2020, 33(19): 8507–8522, https://doi.org/10.1175/ JCLI-D-19-0471.1
- [12] YAO T, BOLCH T, CHEN D, et al. The imbalance of the Asian water tower [J]. Nature Reviews Earth & Environment, 2022, 3(10): 618–632, https://doi.org/10.1038/ s43017-022-00299-4
- [13] YAO T, THOMPSON L G, MOSBRUGGER V, et al. Third Pole Environment (TPE) [J]. Environmental Development, 2012, 3: 52-64, https://doi.org/10.1016/j.envdev.2012.04.002
- [14] CHEN D L, XU B Q, YAO T D, et al. Assessment of past, present and future environmental changes on the Tibetan Plateau [J]. Chinese Science Bulletin, 2015, 60(32): 3025–3035, https://doi.org/10.1360/N972014-01370, in Chinese with English abstract
- [15] CHEN F, ZHANG J, LIU J, et al. Climate change, vegetation history, and landscape responses on the Tibetan Plateau during the Holocene: A comprehensive review [J]. Quaternary Science Reviews, 2020, 243: 106444, https://doi.org/10.1016/j.quascirev.2020.106444
- [16] CHEN L, ZHANG R, PRYOR S C, et al. Influence of wintertime surface sensible heat flux variability over the central and eastern Tibetan Plateau on the East Asian winter monsoon [J]. Climate Dynamics, 2020, 54(11-12): 4589– 4603, https://doi.org/10.1007/s00382-020-05246-x
- [17] DUAN A, SUN R, HE J. Impact of surface sensible heating over the Tibetan Plateau on the western Pacific subtropical high: a land-air-sea interaction perspective [J]. Advances in Atmospheric Sciences, 2017, 34(2): 157–168, https://doi. org/10.1007/s00376-016-6008-z
- [18] DUAN A, WU G. Weakening trend in the atmospheric heat source over the Tibetan Plateau during recent decades, part I: observations [J]. Journal of Climate, 2008, 21(13): 3149– 3164, https://doi.org/10.1175/2007JCLI1912.1
- [19] JIANG X, LI Y, YANG S, et al. Interannual variation of summer atmospheric heat source over the Tibetan Plateau and the role of convection around the Western Maritime Continent [J]. Journal of Climate, 2016, 29(1): 121–138, https://doi.org/10.1175/JCLI-D-15-0181.1
- [20] KUANG X, JIAO J J. Review on climate change on the Tibetan Plateau during the last half century [J]. Journal of Geophysical Research: Atmospheres, 2016, 121(8): 3979– 4007, https://doi.org/10.1002/2015JD024728
- [21] LAI Y, CHEN X, MA Y, et al. Impacts of the westerlies on planetary boundary layer growth over a valley on the north side of the Central Himalayas [J]. Journal of Geophysical Research: Atmospheres, 2021, 126(3): e2020JD033928, https://doi.org/10.1029/2020JD033928
- [22] LIU Y, LU M, YANG H, et al. Land-atmosphere-ocean

- coupling associated with the Tibetan Plateau and its climate impacts [J]. National Science Review, 2020, 7(3): 534–552, https://doi.org/10.1093/nsr/nwaa011
- [23] LIU Y, BAO Q, DUAN A, et al. Recent progress in the impact of the Tibetan Plateau on climate in China [J]. Advances in Atmospheric Sciences, 2007, 24(6): 1060– 1076, https://doi.org/10.1007/s00376-007-1060-3
- [24] WANG X, PANG G, YANG M. Precipitation over the Tibetan Plateau during recent decades: a review based on observations and simulations [J]. International Journal of Climatology, 2018, 38(3): 1116–1131, https://doi.org/ 10.1002/joc.5246
- [25] WANG Z, YANG S, DUAN A, et al. Tibetan Plateau heating as a driver of monsoon rainfall variability in Pakistan [J]. Climate Dynamics, 2019, 52(9-10): 6121–6130, https://doi.org/10.1007/s00382-018-4507-6
- [26] WANG Z, YANG S, LAU N C, et al. Teleconnection between summer NAO and East China rainfall variations: a bridge effect of the Tibetan Plateau [J]. Journal of Climate, 2018, 31(16): 6433–6444, https://doi.org/10.1175/JCLI-D-17-0413.1
- [27] WU G, DUAN A, LIU Y, et al. Tibetan Plateau climate dynamics: recent research progress and outlook [J]. National Science Review, 2015, 2(1): 100–116, https:// doi.org/10.1093/nsr/nwu045
- [28] WU G, XIN L, ZHANG Q, et al. Progresses in the study of the climate impacts of the elevated heating over the Tibetan Plateau [J]. Climatic and Environmental Research, 2002, 7 (2): 184–201, https://doi.org/10.1002/mop.10502
- [29] YE D. Some characteristics of the summer circulation over the Qinghai-Xizang (Tibet) Plateau and its neighborhood
 [J]. Bulletin of the American Meteorological Society, 1981, 62(1): 14–19, https://doi.org/10.1175/1520-0477(1981) 062<0014:SCOTSC>2.0.CO;2
- [30] ZHANG R H, JIANG Z H, GAO X J, et al. An overview of projected climate and environmental changes across the Tibetan Plateau in the 21st century [J]. Chinese Science Bulletin, 2015, 60(32): 3036–3047, https://doi.org/10.1360/ N972014-01296, in Chinese with English abstract
- [31] ZHOU X J, ZHAO P, CHEN J M, et al. Impacts of thermodynamic processes over the Tibetan Plateau on the Northern Hemispheric climate [J]. Science in China Series D: Earth Sciences, 2009, 52: 1679–1693, https://doi.org/ 10.1007/s11430-009-0194-9, in Chinese with English abstract
- [32] CHAN S, XU X D, WANG P J, et al. The warming and wetting ecological environment changes over the Qinghai-Tibetan Plateau and the driving effect of the Asian Summer Monsoon [J]. Journal of Tropical Meteorology, 2022, 28(1): 95–108, https://doi.org/10.46267/j.1006-8775.2022.008
- [33] LI D, YANG K, TANG W, et al. Characterizing precipitation in high altitudes of the western Tibetan plateau with a focus on major glacier areas [J]. International Journal of Climatology, 2020, 40(12): 5114–5127, https://doi.org/10.1002/joc.6509
- [34] LI L, YANG S, WANG Z, et al. Evidence of warming and wetting climate over the Qinghai-Tibet Plateau [J]. Arctic, Antarctic, and Alpine Research, 2010, 42(4): 449–457, https://doi.org/10.1657/1938-4246-42.4.449
- [35] WU Y T, YANG S, HU X M, et al. Difference/similarity

- and attribution of changes in regional summer surface air temperatures over the Tibetan Plateau and its surrounding regions in the past 40 years [J]. Chinese Journal of Atmospheric Sciences, 2022, 46(5): 1253, in Chinese with English abstract
- [36] YANG K, WU H, QIN J, et al. Recent climate changes over the Tibetan Plateau and their impacts on energy and water cycle: a review [J]. Global and Planetary Change, 2014, 112: 79–91, https://doi.org/10.1016/j.gloplacha.2013.12.001
- [37] YOU Q, KANG S, PEPIN N, et al. Climate warming and associated changes in atmospheric circulation in the eastern and central Tibetan Plateau from a homogenized dataset [J]. Global and Planetary Change, 2010, 72(1-2): 11–24, https://doi.org/10.1016/j.gloplacha.2010.04.003
- [38] ARIAS PA, BELLOUIN N, COPPOLA E, et al. Technical Summary [R]. Cambridge and New York: Cambridge University Press, 2023: 33–144, https://doi.org/10.1017/9781009157896.002
- [39] CHEN J, WANG Y, SUN J, et al. Precipitation dominants synergies and trade-offs among ecosystem services across the Qinghai-Tibet Plateau [J]. Global Ecology and Conservation, 2021, 32: e01886, https://doi.org/10.1016/j.gecco.2021.e01886
- [40] CUO L, ZHANG Y. Spatial patterns of wet season precipitation vertical gradients on the Tibetan Plateau and the surroundings [J]. Scientific Reports, 2017, 7(1): 5057, https://doi.org/10.1038/s41598-017-05345-6
- [41] NING B, YANG X, CHANG L. Changes of temperature and precipitation extremes in Hengduan Mountains, Qinghai-Tibet Plateau in 1961–2008 [J]. Chinese Geographical Science, 2012, 22(4): 422–436, https://doi.org/ 10.1007/s11769-012-0549-6
- [42] WANG Z, DUAN A, YANG S, et al. Atmospheric moisture budget and its regulation on the variability of summer precipitation over the Tibetan Plateau [J]. Journal of Geophysical Research: Atmospheres, 2017, 122(2): 614– 630, https://doi.org/10.1002/2016JD025515
- [43] ZHU X, WU T, LI R, et al. Characteristics of the ratios of snow, rain and sleet to precipitation on the Qinghai-Tibet Plateau during 1961–2014 [J]. Quaternary International, 2017, 444: 137–150, https://doi.org/10.1016/j. quaint.2016.07.030
- [44] ZHU Y. A tripole winter precipitation change pattern around the Tibetan Plateau in the late 1990s [J]. Atmospheric and Oceanic Science Letters, 2022, 15(6): 100223, https://doi.org/10.1016/j.aosl.2022.100223
- [45] CHEN Q, GE F, JIN Z, et al. How well do the CMIP6 HighResMIP models simulate precipitation over the Tibetan Plateau? [J]. Atmospheric Research, 2022, 279: 106393, https://doi.org/10.1016/j.atmosres.2022.106393
- [46] CHEN S, HAMDI R, OCHEGE F U, et al. Added value of a dynamical downscaling approach for simulating precipitation and temperature over Tianshan Mountains Area, Central Asia [J]. Journal of Geophysical Research: Atmospheres, 2019, 124(21): 11051–11069, https://doi.org/ 10.1029/2019JD031016
- [47] FU Y H, GAO X J, ZHU Y M, et al. Climate change projection over the Tibetan Plateau based on a set of RCM simulations [J]. Advances in Climate Change Research,

- 2021, 12(3): 313-321, https://doi.org/10.1016/j.ac-cre.2021.01.004
- [48] GAO Y, XUE Y, PENG W, et al. Assessment of dynamic downscaling of the extreme rainfall over East Asia using a regional climate model [J]. Advances in Atmospheric Sciences, 2011, 28(5): 1077–1098, https://doi.org/10.1007/ s00376-010-0039-7
- [49] YOU H, KUN Y, YAO T D, et al. Numerical simulation of a heavy precipitation in Qinghai-Xizang Plateau based on WRF Model [J]. Plateau Meteorology, 2012, 31(5): 1183, in Chinese with English abstract
- [50] LI X F, WU T H, ZHU X F, et al. Improving the Noah MP model for simulating hydrothermal regime of the active layer in the permafrost regions of the Qinghai Tibet Plateau [J]. Journal of Geophysical Research: Atmospheres, 2020, 125(16): e2020JD032588, https://doi.org/2020JD032588
- [51] LIN C, CHEN D, YANG K, et al. Impact of model resolution on simulating the water vapor transport through the central Himalayas: implication for models' wet bias over the Tibetan Plateau [J]. Climate Dynamics, 2018, 51(9-10): 3195–3207, https://doi.org/10.1007/s00382-018-4074-x
- [52] NORRIS J, CARVALHO L M V, JONES C, et al. WRF simulations of two extreme snowfall events associated with contrasting extratropical cyclones over the western and central Himalaya [J]. Journal of Geophysical Research: Atmospheres, 2015, 120(8): 3114–3138, https://doi.org/10.1002/2014JD022592
- [53] OU T, CHEN D, CHEN X, et al. Simulation of summer precipitation diurnal cycles over the Tibetan Plateau at the gray-zone grid spacing for cumulus parameterization [J]. Climate Dynamics, 2020, 54(7-8): 3525–3539, https://doi. org/10.1007/s00382-020-05181-x
- [54] TONG K, SU F, YANG D, et al. Evaluation of satellite precipitation retrievals and their potential utilities in hydrologic modeling over the Tibetan Plateau [J]. Journal of Hydrology, 2014, 519: 423–437, https://doi.org/10.1016/i.jhydrol.2014.07.044
- [55] WANG Y, YANG K, ZHOU X, et al. The formation of a dry - belt in the north side of Central Himalaya Mountains [J]. Geophysical Research Letters, 2019, 46(5): 2993–3000, https://doi.org/10.1029/2018GL081061
- [56] WU S G, LIU Y M, ZOU X L, et al. The simulation analysis of the precipitation over the southern slopes of the Tibetan Plateau based on WRF model [J]. Acta Meteorologica Sinica, 2016, 5: 744–756, https://doi.org/ qxxb2016.048, in Chinese with English abstract
- [57] XU G, XIE Y. Sensitivity of the summer precipitation simulated with WRF model to planetary boundary layer parameterization over the Tibetan Plateau and its downstream areas [J]. Journal of Geology & Geophysics, 2016, 5 (4): 2381–8719, https://doi.org/10.4172/2381-8719.1000249
- [58] YU E, WANG H, GAO Y, et al. Impacts of cumulus convective parameterization schemes on summer monsoon precipitation simulation over China [J]. Acta Meteorologica Sinica, 2011, 25(5): 581–592, https://doi.org/10.1007/s13351-011-0504-y
- [59] NIU X, TANG J, CHEN D, et al. The performance of

- CORDEX-EA-II simulations in simulating seasonal temperature and elevation-dependent warming over the Tibetan Plateau [J]. Climate Dynamics, 2021, 57(3-4): 1135–1153, https://doi.org/10.1007/s00382-021-05760-6
- [60] PEPIN N, BRADLEY R S, DIAZ H F, et al. Elevation-dependent warming in mountain regions of the world [J]. Nature Climate Change, 2015, 5(5): 424–430, https://doi.org/10.1038/nclimate2563
- [61] BAI L, WEN Y, SHI C, et al. Which precipitation product works best in the Qinghai-Tibet Plateau, multi-source blended data, global/regional reanalysis data, or satellite retrieved precipitation data? [J]. Remote Sensing, 2020, 12 (4): 683, https://doi.org/10.3390/rs12040683
- [62] LIU J, SHANGGUAN D, LIU S, et al. Evaluation and comparison of CHIRPS and MSWEP daily-precipitation products in the Qinghai-Tibet Plateau during the period of 1981–2015 [J]. Atmospheric Research, 2019, 230: 104634, https://doi.org/10.1016/j.atmosres.2019.104634
- [63] LIU J, SHANGUAN D, LIU S, et al. Evaluation and hydrological simulation of CMADS and CFSR Reanalysis datasets in the Qinghai-Tibet Plateau [J]. Water, 2018, 10 (4): 513, https://doi.org/10.3390/w10040513
- [64] WANG A H, ZENG X N. Evaluation of multireanalysis products with in situ observations over the Tibetan Plateau [J]. Journal of Geophysical Research: Atmospheres, 2012, 117: D05102, https://doi.org/10.1029/2011JD016553
- [65] XUE J, XIAO Z, BROMWICH D H, et al. Polar WRF V4.1.1 simulation and evaluation for the Antarctic and Southern Ocean [J]. Frontiers of Earth Science, 2022, 16(4): 1005–1024, https://doi.org/10.1007/s11707-022-0971-8
- [66] XUE J, BROMWICH D H, XIAO Z, et al. Impacts of initial conditions and model configuration on simulations of polar lows near Svalbard using Polar WRF with 3DVAR [J]. Quarterly Journal of the Royal Meteorological Society, 2021, 147(740): 3806–3834, https://doi.org/10.1002/qj.4158
- [67] BROMWICH D H, WILSON A B, BAI L, et al. The Arctic System Reanalysis, Version 2 [J]. Bulletin of the American Meteorological Society, 2018, 99(4): 805–828, https://doi. org/10.1175/BAMS-D-16-0215.1
- [68] BROMWICH D H, OTIENO F O, HINES K M, et al. Comprehensive evaluation of polar weather research and forecasting model performance in the Antarctic [J]. Journal of Geophysical Research: Atmospheres, 2013, 118(2): 274– 292, https://doi.org/10.1029/2012JD018139
- [69] BROMWICH D H, HINES K M, BAI L S. Development and testing of Polar Weather Research and Forecasting model: 2 Arctic Ocean [J]. Journal of Geophysical Research: Atmospheres, 2009, 114(D8): 10.1029– 2008JD010300, https://doi.org/10.1029/2008JD010300
- [70] HINES K M, BROMWICH D H, BAI L S, et al. Development and testing of Polar WRF, Part III: arctic land [J]. Journal of Climate, 2011, 24(1): 26–48, https://doi. org/10.1175/2010JCLI3460.1
- [71] HINES K M, BROMWICH D H. Development and testing of Polar Weather Research and Forecasting (WRF) Model Part I: greenland ice sheet meteorology [J]. Monthly Weather Review, 2008, 136(6): 1971–1989, https://doi. org/10.1175/2007MWR2112.1
- [72] WILSON A B, BROMWICH D H, HINES K M.

- Evaluation of Polar WRF forecasts on the Arctic System Reanalysis Domain: 2 atmospheric hydrologic cycle [J]. Journal of Geophysical Research: Atmospheres, 2012, 117 (D4): 2011JD016765, https://doi.org/10.1029/2011JD016765
- [73] WILSON A B, BROMWICH D H, HINES K M. Evaluation of Polar WRF forecasts on the Arctic System Reanalysis domain: Surface and upper air analysis [J]. Journal of Geophysical Research, 2011, 116(D11): D11112, https://doi.org/10.1029/2010JD015013
- [74] KUMAR A, ROY BHOWMIK S K, DAS A K. Implementation of Polar WRF for short range prediction of weather over Maitri region in Antarctica [J]. Journal of Earth System Science, 2012, 121(5): 1125–1143, https://doi.org/10.1007/s12040-012-0217-3
- [75] POWERS J G, KLEMP J B, SKAMAROCK W C, et al. The Weather Research and Forecasting Model: overview, system efforts, and future directions [J]. Bulletin of the American Meteorological Society, 2017, 98(8): 1717–1737, https://doi.org/10.1175/BAMS-D-15-00308.1
- [76] POWERS J G, MANNING K W, BROMWICH D H, et al. A decade of Antarctic science support through AMPS [J]. Bulletin of the American Meteorological Society, 2012, 93 (11): 1699–1712, https://doi.org/10.1175/BAMS-D-11-00186.1
- [77] WALSH J E, BROMWICH D H, OVERLAND J E, et al. 100 years of progress in polar meteorology [J]. Meteorological Monographs, 2018, 59: 21.1–21.36, https://doi.org/10.1175/AMSMONOGRAPHS-D-18-0003.1
- [78] HINES K M, BROMWICH D H, WANG S H, et al. Microphysics of summer clouds in central west Antarctica simulated by Polar WRF and AMPS [J]. Atmospheric Chemistry and Physics Discussions, 2019: 1–48, https://doi. org/10.5194/acp-2018-1251
- [79] HINES K M, BROMWICH D H, BAI L, et al. Sea ice enhancements to Polar WRF [J]. Monthly Weather Review, 2015, 143(6): 2363–2385, https://doi.org/10.1175/MWR-D-14-00344.1
- [80] HINES K M, BROMWICH D H. Simulation of Late Summer Arctic Clouds during ASCOS with Polar WRF [J]. Monthly Weather Review, 2017, 145(2): 521–541, https://doi.org/10.1175/MWR-D-16-0079.1
- [81] SKAMAROCK C, KLEMP B, DUDHIA J, et al. A description of the advanced research WRF Model Version 4.1 [R]. 2019, https://doi.org/10.5065/1dfh-6p97
- [82] CAO Q, YU D, GEORGESCU M, et al. Impacts of land use and land cover change on regional climate: a case study in the agro-pastoral transitional zone of China [J]. Environmental Research Letters, 2015, 10(12): 124025, https://doi.org/10.1088/1748-9326/10/12/124025
- [83] LI D, TIAN P, LUO H, et al. Impacts of land use and land cover changes on regional climate in the Lhasa River basin, Tibetan Plateau [J]. Science of The Total Environment, 2020, 742: 140570, https://doi.org/10.1016/j.scitoteny.2020.140570
- [84] LI H, ZHANG H, MAMTIMIN A, et al. A new land-use dataset for the Weather Research and Forecasting (WRF) Model [J]. Atmosphere, 2020, 11(4): 350, https://doi.org/ 10.3390/atmos11040350

- [85] LI X, MITRA C, DONG L, et al. Understanding land use change impacts on microclimate using Weather Research and Forecasting (WRF) model [J]. Physics and Chemistry of the Earth, Parts A/B/C, 2018, 103: 115–126, https://doi.org/10.1016/j.pce.2017.01.017
- [86] NAHIAN M R, NAZEM A, NAMBIAR M K, et al. Complex meteorology over a complex mining facility: assessment of topography, land use, and grid spacing modifications in WRF [J]. Journal of Applied Meteorology and Climatology, 2020, 59(4): 769–789, https://doi.org/ 10.1175/JAMC-D-19-0213.1
- [87] SCHICKER I, ARNOLD ARIAS D, SEIBERT P. Influences of updated land-use datasets on WRF simulations for two Austrian regions [J]. Meteorology and Atmospheric Physics, 2016, 128(3): 279–301, https://doi.org/10.1007/s00703-015-0416-y
- [88] TEKLAY A, DILE Y T, ASFAW D H, et al. Impacts of land surface model and land use data on WRF model simulations of rainfall and temperature over Lake Tana Basin, Ethiopia [J]. Heliyon, 2019, 5(9): e02469, https://doi.org/10.1016/j.heliyon.2019.e02469
- [89] YIN K, XU S, ZHAO Q, et al. Effects of land cover change on atmospheric and storm surge modeling during typhoon event [J]. Ocean Engineering, 2020, 199: 106971, https:// doi.org/10.1016/j.oceaneng.2020.106971
- [90] FARR T G, ROSEN P A, CARO E, et al. The shuttle radar topography mission [J]. Reviews of Geophysics, 2007, 45 (2): 2005RG000183, https://doi.org/10.1029/ 2005RG000183
- [91] DE MEIJ A, VINUESA J F. Impact of SRTM and Corine Land Cover data on meteorological parameters using WRF [J]. Atmospheric Research, 2014, 143: 351–370, https://doi.org/10.1016/j.atmosres.2014.03.004
- [92] XU E Q. Land use of the Tibet Plateau in 2015 (Version 1.0) [R]. National Tibetan Plateau/Third Pole Environment Data Center, 2019, https://doi.org/10.11888/Geogra. tpdc.270198
- [93] BROMWICH D H, BAI L, BJARNASON G G. Highresolution regional climate simulations over Iceland using Polar MM5 [J]. Monthly Weather Review, 2005, 133(12): 3527–3547, https://doi.org/10.1175/MWR3049.1
- [94] IACONO M J, DELAMERE J S, MLAWER E J, et al. Radiative forcing by long - lived greenhouse gases: calculations with the AER radiative transfer models [J]. Journal of Geophysical Research: Atmospheres, 2008, 113(D13): 2008JD009944, https://doi.org/10.1029/2008JD009944
- [95] DEE D P, UPPALA S M, SIMMONS A J, et al. The ERA - Interim reanalysis: configuration and performance of the data assimilation system [J]. Quarterly Journal of the Royal Meteorological Society, 2011, 137(656): 553–597, https://doi.org/10.1002/qj.828
- [96] HERSBACH H, BELL B, BERRISFORD P, et al. The ERA5 global reanalysis [J]. Quarterly Journal of the Royal Meteorological Society, 2020, 146(730): 1999–2049, https://doi.org/10.1002/qj.3803
- [97] GAO Y, CHEN F, JIANG Y. Evaluation of a convectionpermitting modeling of precipitation over the Tibetan Plateau and its influences on the simulation of snow-cover fraction [J]. Journal of Hydrometeorology, 2020, 21(7):

- 1531-1548, https://doi.org/10.1175/JHM-D-19-0277.1
- [98] HEATH N K, FUELBERG H E. Using a WRF simulation to examine regions where convection impacts the Asian summer monsoon anticyclone [J]. Atmospheric Chemistry and Physics, 2014, 14(4): 2055–2070, https://doi.org/10.5194/acp-14-2055-2014
- [99] GLISAN J M, GUTOWSKI WILLIAM J J, CASSANO J J, et al. Effects of Spectral Nudging in WRF on Arctic Temperature and Precipitation Simulations [J]. Journal of Climate, 2013, 26(12): 3985–3999, https://doi.org/10.1175/ JCLI-D-12-00318.1
- [100] CHA D H, JIN C S, LEE D K, et al. Impact of intermittent spectral nudging on regional climate simulation using Weather Research and Forecasting model [J]. Journal of Geophysical Research, 2011, 116(D10): D10103, https://doi.org/10.1029/2010JD015069
- [101] LIU P, TSIMPIDI A P, HU Y, et al. Differences between downscaling with spectral and grid nudging using WRF [J]. Atmospheric Chemistry and Physics, 2012, 12(8): 3601–3610, https://doi.org/10.5194/acp-12-3601-2012
- [102] OTTE T L, NOLTE C G, OTTE M J, et al. Does nudging squelch the extremes in regional climate modeling? [J]. Journal of Climate, 2012, 25(20): 7046–7066, https://doi.org/10.1175/JCLI-D-12-00048.1
- [103] VON STORCH H, LANGENBERG H, FESER F. A spectral nudging technique for dynamical downscaling purposes [J]. Monthly Weather Review, 2000, 128(10): 3664–3673, https://doi.org/10.1175/1520-0493(2000) 128<3664:ASNTFD>2.0.CO;2
- [104] CHEN X, PAULUIS O M, ZHANG F. Regional simulation of Indian summer monsoon intraseasonal oscillations at gray-zone resolution [J]. Atmospheric Chemistry and Physics, 2018, 18(2): 1003–1022, https://doi.org/10.5194/acp-18-1003-2018
- [105] GAO Y, CHEN F, MIGUEZ-MACHO G, et al. Understanding precipitation recycling over the Tibetan Plateau using tracer analysis with WRF [J]. Climate Dynamics, 2020, 55(9-10): 2921–2937, https://doi.org/10.1007/s00382-020-05426-9
- [106] QIAN T, ZHANG F, WEI J, et al. Diurnal characteristics of gravity waves over the Tibetan Plateau in 2015 summer using 10-km downscaled simulations from WRF-EnKF Regional Reanalysis [J]. Atmosphere, 2020, 11(6): 631, https://doi.org/10.3390/atmos11060631
- [107] ZHENG Y, ALAPATY K, HERWEHE J A, et al. Improving high-resolution weather forecasts using the Weather Research and Forecasting (WRF) Model with an Updated Kain–Fritsch Scheme [J]. Monthly Weather Review, 2016, 144(3): 833–860, https://doi.org/10.1175/ MWR-D-15-0005.1
- [108] GRELL G A, DÉVÉNYI D. A generalized approach to parameterizing convection combining ensemble and data assimilation techniques [J]. Geophysical Research Letters, 2002, 29(14): 1693, https://doi.org/10.1029/2002GL015311
- [109] KAIN J S. The Kain–Fritsch convective parameterization: an update [J]. Journal of Applied Meteorology, 2004, 43 (1): 170–181, https://doi.org/10.1175/1520-0450(2004) 043<0170:TKCPAU>2.0.CO;2

- [110] NAKANISHI M, NIINO H. Development of an improved turbulence closure model for the atmospheric boundary layer [J]. Journal of the Meteorological Society of Japan, 2009, 87(5): 895–912, https://doi.org/10.2151/jmsj.87.895
- [111] HONG S Y, NOH Y, DUDHIA J. A new vertical diffusion package with an explicit treatment of entrainment processes [J]. Monthly Weather Review, 2006, 134(9): 2318–2341, https://doi.org/10.1175/MWR3199.1
- [112] OLSON J B, KENYON J S, ANGEVINE W A, et al. A description of the MYNN-EDMF scheme and the coupling to other components in WRF-ARW [R]. NOAA, 2019, https://repository.library.noaa.gov/view/noaa/19837
- [113] BAUER P, THORPE A, BRUNET G. The quiet revolution of numerical weather prediction [J]. Nature, 2015, 525 (7567): 47–55, https://doi.org/10.1038/nature14956
- [114] BENJAMIN S G, BROWN J M, BRUNET G, et al. 100 years of progress in forecasting and NWP applications [J]. Meteorological Monographs, 2019, 59: 13.1–13.67, https://doi.org/10.1175/amsmonographs-d-18-0020.1
- [115] RANDALL D A, BITZ C M, DANABASOGLU G, et al. 100 Years of Earth System Model Development [J]. Meteorological Monographs, 2019, 59: 12.1–12.66, https://doi.org/10.1175/amsmonographs-d-18-0018.1
- [116] ZHU G L, WANTAO L I N, YANHUA C A O. Numerical simulation of a rainstorm event over South China by using various cloud microphysics parameterization schemes in WRF model and its performance analysis [J]. Chinese Journal of Atmospheric Sciences, 2014, 38(3): 513–523, https://doi.org/10.3878/j.issn.1006-9895.2013.13202, in Chinese with English abstract
- [117] LI Z, MA Z S, LIU J L, et al. The improvement of GRAPES double moment cloud scheme and case study of cloud precipitation: modeling study of tropical convective cloud via GRAPES_SCM [J]. Meteorological Monthly, 2019, 45(6): 756–765
- [118] M N, OU T H, LIU D Q, et al. Summer regional climate simulations over Tibetan Plateau: from gray zone to convection permitting scale [J]. Climate Dynamics, 2022, 60(1): 301-322.
- [119] SHEN X Y, SHI Y S, WANG H, et al. Comparison of two double-moment cloud microphysics schemes in the GRAPES_Meso model on simulating a cold cloud process [J]. Torrential Rain and Disasters, 2022, 41(3): 336-347, https://doi.org/10.3969/j.issn.1004-9045.2022.03.010, in Chinese with English abstract
- [120] YANG Y, BING L, WEI W, et al. Impacts of cumulus parameterization schemes on the summertime precipitation forecast in China based on the WRF model [J]. Acta Meteorologica Sinica, 2021, 79(4): 612–625, https://doi.org/10.11676/qxxb2021.045, in Chinese with English abstract
- [121] ZHANG M, WANG H, ZHANG X, et al. Applying the WRF Double-Moment Six-Class Microphysics Scheme in the GRAPES_Meso Model: a case study [J]. Journal of Meteorological Research, 2018, 32(2): 246–264, https:// doi.org/10.1007/s13351-018-7066-1
- [122] YAN Y, LIU Y, LIU X, et al. Effects of cloud microphysics on the vertical structures of cloud radiative effects over the tibetan plateau and the Arctic [J]. Remote Sensing, 2021, 13(14): 2651, https://doi.org/10.3390/

rs13142651

- [123] MORRISON H, MILBRANDT J A. Parameterization of Cloud microphysics based on the prediction of bulk ice particle properties, Part I: scheme description and idealized tests [J]. Journal of the Atmospheric Sciences, 2015, 72(1): 287–311, https://doi.org/10.1175/JAS-D-14-0065.1
- [124] THOMPSON G, EIDHAMMER T. A study of aerosol impacts on clouds and precipitation development in a large winter cyclone [J]. Journal of the Atmospheric Sciences, 2014, 71(10): 3636–3658, https://doi.org/10.1175/JAS-D-13-0305.1
- [125] LIM K S S, HONG S Y. Development of an effective double-moment cloud microphysics scheme with prognostic Cloud Condensation Nuclei (CCN) for weather and climate models [J]. Monthly Weather Review, 2010, 138 (5): 1587–1612, https://doi.org/10.1175/2009MWR2968.1
- [126] HUANG L P, CHEN D H, DENG L T, et al. Main technical improvements of GRAPES_Meso V4.0 and verification [J]. Journal of Appled Meteorological Science, 2017, 28(1): 25–37, https://doi.org/10.11898/1001-7313.20170103, in Chinese with English abstract
- [127] MA Z, HAN W, ZHAO C, et al. A case study of evaluating the GRAPES_Meso V5.0 forecasting performance utilizing observations from South China Sea Experiment 2020 of the "Petrel Project" [J]. Atmospheric Research, 2022, 280: 106437, https://doi.org/10.1016/j. atmosres.2022.106437
- [128] China Meteorological Data Network. Daily precipitation on the Tibetan Plateau and its surrounding areas (1979-2015) [Z]. The National Tibetan Plateau/Third Pole Environment Data Center, 2019
- [129] HUFFMAN G J, BOLVIN D T, NELKIN E J, et al. The TRMM Multisatellite Precipitation Analysis (TMPA): quasi-global, multiyear, combined-sensor precipitation estimates at fine scales [J]. Journal of Hydrometeorology, 2007, 8(1): 38–55, https://doi.org/10.1175/JHM560.1
- [130] LI C, ZHAO T, SHI C, et al. Evaluation of daily precipitation product in China from the CMA Global Atmospheric Interim Reanalysis [J]. Journal of Meteorological Research, 2020, 34(1): 117–136, https://doi.org/ 10.1007/s13351-020-8196-9
- [131] SHEN C, ZHA J, WU J, et al. Does CRA-40 outperform other reanalysis products in evaluating near-surface wind speed changes over China? [J]. Atmospheric Research, 2022, 266: 105948, https://doi.org/10.1016/j.atmosres.2021.105948
- [132] YANG J, HUANG M, ZHAI P. Performance of the CRA-40/Land, CMFD, and ERA-Interim Datasets in reflecting changes in surface air temperature over the Tibetan Plateau [J]. Journal of Meteorological Research, 2021, 35 (4): 663–672, https://doi.org/10.1007/s13351-021-0196-x
- [133] YU X, ZHANG L, ZHOU T, et al. The Asian Subtropical Westerly jet stream in CRA-40, ERA5, and CFSR Reanalysis Data: comparative assessment [J]. Journal of Meteorological Research, 2021, 35(1): 46–63, https://doi.

- org/10.1007/s13351-021-0107-1
- [134] ZHANG J, ZHAO T, LI Z, et al. Evaluation of surface relative humidity in China from the CRA-40 and current reanalyses [J]. Advances in Atmospheric Sciences, 2021, 38(11): 1958–1976, https://doi.org/10.1007/s00376-021-0333-6
- [135] JIANG X, YUAN H, XUE M, et al. Analysis of a heavy rainfall event over Beijing during 21–22 July 2012 based on high resolution model analyses and forecasts [J]. Journal of Meteorological Research, 2014, 28(2): 199–212, https://doi.org/10.1007/s13351-014-3139-y
- [136] MESINGER F. Bias adjusted precipitation threat scores [J]. Advances in Geosciences, 2008, 16: 137–142, https://doi.org/10.5194/adgeo-16-137-2008
- [137] YANG M J, TUNG Q C. Evaluation of rainfall forecasts over Taiwan by four cumulus parameterization schemes [J]. Journal of the Meteorological Society of Japan, 2003, 81(5): 1163–1183, https://doi.org/10.2151/jmsj.81.1163
- [138] MIGUEZ-MACHO G, STENCHIKOV G L, ROBOCK A. Spectral nudging to eliminate the effects of domain position and geometry in regional climate model simulations [J]. Journal of Geophysical Research: Atmospheres, 2004, 109(D13): 10.1029–2003JD004495, https:// doi.org/10.1029/2003JD004495
- [139] BOWDEN J H, OTTE T L, NOLTE C G, et al. Examining interior grid nudging techniques using two-way nesting in the WRF model for regional climate modeling [J]. Journal of Climate, 2012, 25(8): 2805–2823, https://doi.org/10.1175/JCLI-D-11-00167.1
- [140] WOOTTEN A, BOWDEN J H, BOYLES R, et al. The sensitivity of WRF downscaled precipitation in Puerto Rico to cumulus parameterization and interior grid nudging [J]. Journal of Applied Meteorology and Climatology, 2016, 55(10): 2263–2281, https://doi.org/10.1175/JAMC-D-16-0121.1
- [141] MAI X P, MA Y Y, YANG Y I, et al. Impact of grid nudging parameters on dynamical downscaling during Summer over mainland China [J]. Atmosphere, 2017, 8 (10): 184, https://doi.org/10.3390/atmos8100184
- [142] SPERO T L, OTTE M J, BOWDEN J H, et al. Improving the representation of clouds, radiation, and precipitation using spectral nudging in the Weather Research and Forecasting model [J]. Journal of Geophysical Research: Atmospheres, 2014, 119(20): 11,682–11,694, https://doi. org/10.1002/2014JD022173
- [143] HONG S Y. Hongandlim-JKMS-2006 [J]. Journal of the Korean Meteorological Society, 2006, 42: 129–151
- [144] LI Z Q. Impacts of Thermal Contrast Between the Tibetan Plateau and Indian Ocean on the South Asian Monsoon and Water Vapor Transport [D]. Beijing: University of Chinese Academy of Sciences, 2021, in Chinese with English abstract
- [145] JEWORREK J, WEST G, STULL R. WRF precipitation performance and predictability for systematically varied parameterizations over complex Terrain [J]. Weather and Forecasting, 2021, 36(3): 893–913, https://doi.org/10.1175/WAF-D-20-0195.1